Review

Recent Advances in Surface Modifications of Elemental Two-Dimensional Materials: Structures, Properties, and Applications

Junbo Chen[1], Chenhui Wang[1], Hao Li[2], Xin Xu[3], Jiangang Yang[2], Zhe Huo[1], Lixia Wang[1], Weifeng Zhang[1,*], Xudong Xiao[2,*] and Yaping Ma[1,*]

[1] Key Laboratory of Quantum Matt Science, Henan Key Laboratory of Photovoltaic Materials, Henan University, Zhengzhou, Henan 450046, People's Republic of China
[2] School of Physical Science and Technology and Key Laboratory of Artificial Micro- and Nano-Structures of Ministry of Education, Wuhan University, Wuhan, Hubei 430072, People's Republic of China
[3] State Key Lab of Optoelectronic Materials and Technologies, Guangdong Province Key Laboratory of Display Material and Technology, School of Electronics and Information Technology, Sun Yat-sen University, Guangzhou, Guangdong 510275, People's Republic of China
* Correspondence: mustc@henu.edu.cn (Y.M.); xdxiao@whu.edu.cn (X.X.); wfzhang6@163.com (W.Z.)

Abstract: The advent of graphene opens up the research into two-dimensional (2D) material, which is considered as a revolutionary material in the future. Due to its unique geometric structure, graphene exhibits a series of exotic physical and chemical properties. Besides, single-element-based 2D materials (Xenes) have garnered tremendous interest. At present, 16 kinds of Xenes (silicene, borophene, germanene, phosphorene, tellurene, etc.) have been explored, mainly distributed in the third, fourth, fifth and sixth main groups. The current methods to prepare monolayer or few-layer 2D materials include epitaxy growth, mechanical exfoliation, and liquid phase exfoliation. Although two Xenes (aluminene and indiene) have not been synthesized due to the limitations of synthetic methods or stability of Xenes, other Xenes have been successfully realized by elaborately artificial design and synthesis. Focusing on elemental 2D materials, this review mainly summarizes the recently reported work about tuning the electronic, optical, mechanical, or chemical properties of Xenes *via* surface modifications achieved by controllable approaches (doping, adsorption, strain, intercalation, phase transition, etc.) to broaden the applications in various fields, including spintronics, electronics, optoelectronics, superconducting, photovoltaics, sensors, catalysis, and biomedicines. These advances in surface modification of Xenes have laid a theoretical and experimental foundation for the development of 2D materials and their practical applications in diverse fields.

Keywords: elemental two-dimensional materials; allotropic structures; surface modifications; properties; applications

1. Introduction

Graphene, initially isolated from graphite by mechanical exfoliation, possesses a layered honeycomb structure and exhibits fascinating electrical and thermal properties [1]. Subsequently, two-dimensional (2D) materials, including elemental monolayers (Xenes) [2], transition metal chalcogenides (TMCs) [3, 4], oxides [5], halides [6, 7], and carbides (MXenes) [8, 9], have shown intriguing properties, such as high carrier mobility [10], layer-dependent band structures and magnetic properties [6, 11, 12], nontrivial topology [13-16], valleytronics [17], etc. Therefore, 2D materials have become promising candidates for various applications relating to next-generation technology, including spintronics, superconducting, nanoelectronics, nanosensing, etc.

Over the past few years, many researches have focused on searching for other 2D Xenes with distinctive and exciting properties beyond graphene (Figure 1a) [18, 19]. The

Preprints (www.preprints.org) | NOT PEER-REVIEWED | Posted: 14 December 2022 doi:10.20944/preprints202212.0247.v1

successful experimental realization of non-graphene 2D analogs (silicene and phosphorene) sparked a continuous expansion of the list of elements in atomically thin form [20, 21]. 16 elemental main group 2D Xenes have been predicted theoretically or realized experimentally to date (Figure 1b) [22-32]. To the best of our knowledge, except aluminene and indiene, other 13 non-graphene Xenes have experimentally obtained (Figure 1c). Currently, monolayer or few-layer Xenes can be achieved by mechanical exfoliation, liquid phase exfoliation and epitaxial growth methods [1, 12, 22, 33].

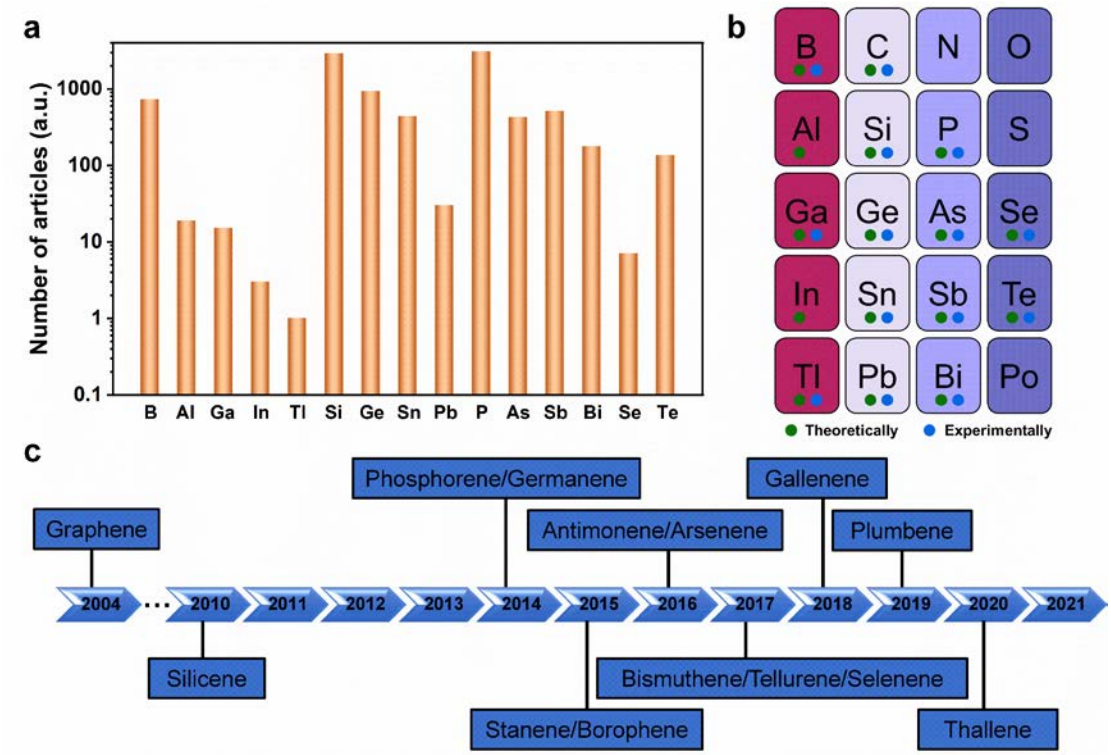

Figure 1. Development of 2D Xenes. (a) Statistics diagram of Number of research articles of non-graphene 2D Xenes from 2010 to 2021. (b) Overview of 2D analogues of main-group elements, explored by either experimental or theoretical routes. The elements with no signs have not been explored to date. (c) The timeline of experimental realization of 2D Xenes.

Even though 2D Xenes have demonstrated great potentials in numerous applications, their intrinsic properties usually constrain the expansion of applications. For instance, despite the high mobility, the gapless band structure in graphene restricts its applications in electronic devices. Therefore, fine-tuning the properties of 2D Xenes plays an essential role in overcoming their intrinsic constraints [34-37]. Surface modifications can effectively tailor the properties of 2D Xenes for practical applications. The common approaches for surface modifications include heteroatom doping [38, 39], adsorption [34, 36, 40], in-plane heterostructure formation [41-43], boundary formation [44], edge shape [32, 45-48], phase transition [49], strain [50, 51], twisted structure [52, 53], etc. Motivated by recent advances in surface modifications of 2D Xenes, herein we review the reported work to date, connect the surface modifications of various 2D Xenes to their measured/predicted properties, and evaluate their advantages and disadvantages for various applications.

2. Classification of 2D Xenes

The material properties (electronic, optical, chemical, etc.) of 2D Xenes are not only determined by their chemical composition, but also are strongly associated to the atom arrangement in the lattice. Due to the preferred orbital hybridization for various elements in main group, 2D Xenes have been theoretically predicted or experimentally verified to

 doi:10.20944/preprints202212.0247.v1

possess allotropes with diverse crystal lattices (Figure 2). The reported 16 Xenes are classified by main groups, including: group III (borophene, aluminene, gallenene, indiene, and thallene); group IV (graphene, silicene, germanene, stanene, and plumbene); group V (phosphorene, arsenene, antimonene, and bismuthene); and group VI (selenene, and tellurene).

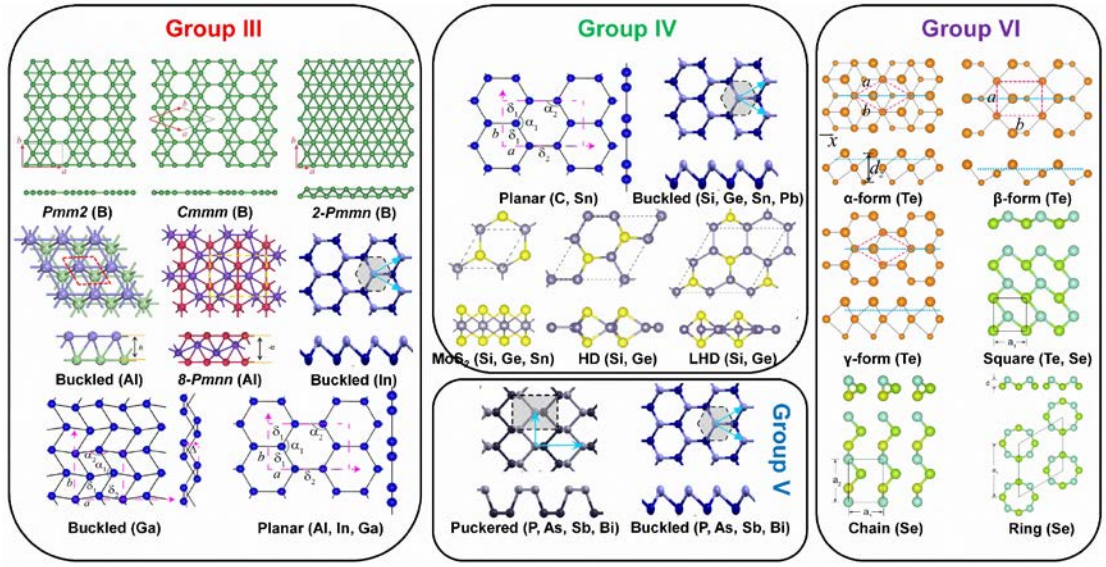

Figure 2. Allotropes of various 2D Xenes in main groups predicted theoretically or realized experimentally. Allotropes of borophene: Reproduced with permission from ref. [54]. Copyright 2017 Informa UK Limited, trading as Taylor & Francis Group. Allotropes of aluminene: Reproduced with permission from ref. [55]. Copyright 2017 Elsevier Ltd. Allotropes of gallenene: Reproduced with permission from ref. [29]. Copyright 2018 American Association for the Advancement of Science. Buckled and Puckered structures: Reproduced with permission from ref. [56]. Copyright 2016 American Physical Society. MoS_2-like, HD, and LHD structures: Reproduced with permission from ref. [57]. Copyright 2015 American Physical Society. α-form, β-form and γ-form of tellurene: Reproduced with permission from ref. [27]. Copyright 2017 American Physical Society. Square-, chain-, and ring-Se: Reproduced with permission from ref. [58]. Copyright 2017 IOP Publishing.

In group III elements, theoretical calculations have predicted many allotropes of 2D borophene ($B_{1-v}\square_v$, v presents vacancy concentration) with various vacancy concentrations and 2D aluminene with various forms [55, 59-61]. However, only two allotropes of 2D gallenene (buckled and planar structures) have been successfully exfoliated [29]. Similarly, 2D indiene has been predicted to possess a buckled, a planar as well as a puckered geometry [62]. Among group IV elements, the favorable hybridization state is somewhere between sp^2 and sp^3, leading to various 2D allotropic structures, like planar honeycomb graphene/stanene [63-65], buckled silicene/germanene/stanene/plumbene [25, 30, 66, 67], pha-/penta-graphene [68, 69], MoS_2-like stanene [57], honeycomb dumbbell (HD)/large honeycomb dumbbell (LHD) silicene/germanene [57]. Different from group III and group IV, all the elements in group V prefer the sp^3 hybridization state to create buckled (α-form) or puckered (β-form) lattice [24, 70-75]. Meanwhile, a γ-form and a δ-form of arsenene has also been proposed [56]. In group VI, four different allotropic forms of tellurene have been predicted [27, 58], while Se can form a chain, a ring, or a square structure [58]. To verify the atomic structures of various elemental Xenes, epitaxial growth has been attempted on many substrates, analogous to the epitaxial growth of graphene. The suitable substrates for epitaxial growth of various non-graphene Xenes (Figure 3) reveals that the substrate choices affect whether the synthesis can success in addition to the allotropic lattice structure.

Preprints (www.preprints.org) | NOT PEER-REVIEWED | Posted: 14 December 2022 doi:10.20944/preprints202212.0247.v1

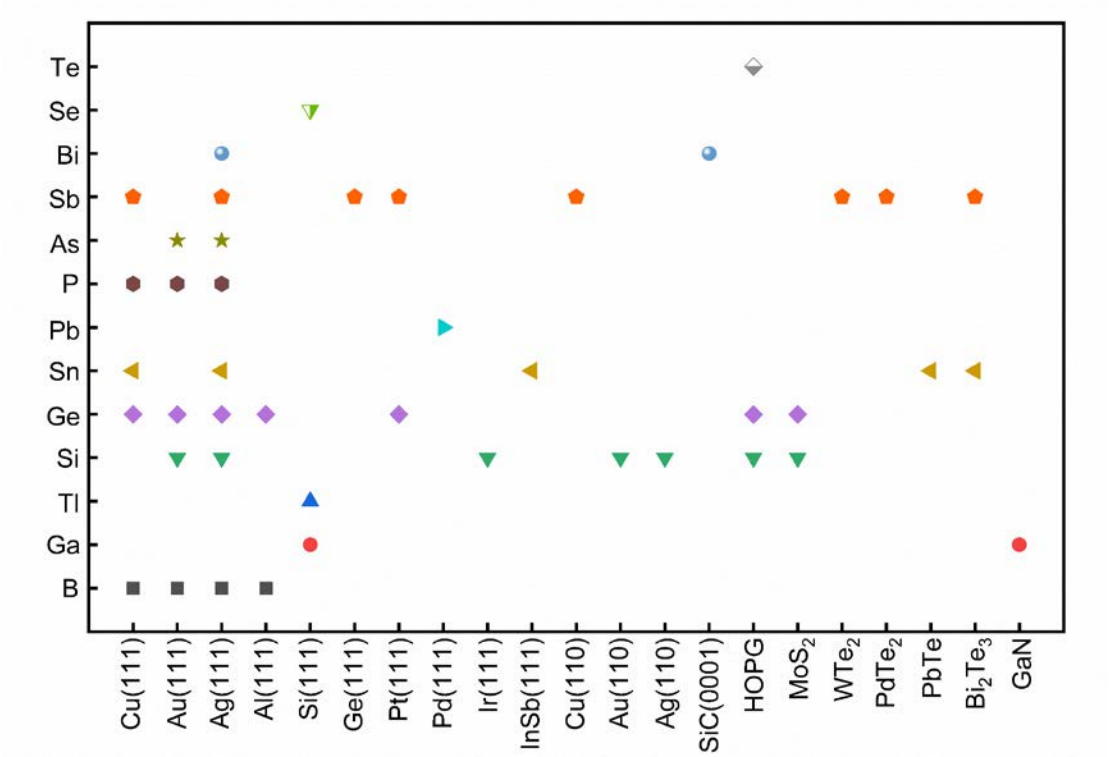

Figure 3. Summary of the successful substrate choices for the epitaxial growth of various non-graphene 2D Xenes.

3. Surface modifications of 2D Xenes in various main groups

3.1. Group III

Borophene. Borophene, monolayer of boron atoms, has been synthesized on many metal substrates under ultrahigh-vacuum condition [22, 76-78]. Several phases of borophenes, including 2-*Pmmn*, $\nu_{1/6}$ (β_{12}), $\nu_{1/5}$ (χ_3), $\nu_{1/12}$, and honeycomb, which are realized experimentally, exhibit metallic properties [22, 76-78]. However, plenty of borophene allotropes with various vacancy concentrations have been reported by theoretical calculations [59, 60, 79-81]. Moreover, the relationship between the formation energy and vacancy concentration shows a V-shaped function [82], demonstrating the vacancy concentration is directly correlated with the stability of borophene.

Borophene possesses some unique physical and chemical properties. Due to the strong B-B bonds and distinctive atomic structure, borophene exhibits ultrahigh mechanical modulus [83, 84]. The Young's modulus of *Pmmm* and 2-*Pmmn* phases of borophene along armchair direction can reach 574.61 and 398 N m^{-1}, respectively, larger than that of graphene. In fact, several factors, including vacancy concentration, chemical modification, the layer numbers, and temperature, can affect the mechanical properties of borophene. The Young's modulus of borophene was found to decrease with increasing vacancy concentration, layer numbers, and temperature as well as hydrogenation or fluorination [83-89]. Because of its outstanding flexibility and excellent electronic conductivity, borophene has a wide range of intriguing applications in flexible electronic devices [79]. In addition, the thermal conductivity of 2-*Pmmn* phase of borophene is different along the zigzag and armchair directions due to the highly anisotropic atomic structure [90, 91]. The electronic band structures of borophene show 1D nearly free electron states and metallic Dirac fermions [92-95]. However, the metallic-to-semiconducting transition can be achieved by fluorination, and a uniaxial or biaxial strain [85, 96, 97]. At last but not least, the superconductivity of borophene is the most notable characteristic, sparking plenty of research interest [80, 98-106]. The superconducting transition temperatures (T_c) can be tuned by vacancy concentration, doping, strain, and Mg intercalation. T_c exhibits a V-shaped function

 doi:10.20944/preprints202212.0247.v1

as the hexagon hole density [99], illustrating that T_c gradually decreases with rising boron vacancy concentration up to $\nu = 1/9$; thereafter, T_c steadily increases with vacancy concentration. Furthermore, a tensile strain or hole-doping can increase T_c, in contrast, a compressive strain or electron-doping decreases T_c [106]. The suppression induced by electron-doping makes it difficult to experimentally probe superconductivity in substrate-supported borophene.

The physical and chemical properties of borophene can be tuned by surface modifications, such as hydrogenation, fluorination, doping, intercalation, strain, etc. The Young's modulus of borophene decreases after hydrogenation or fluorination. Furthermore, hydrogenation can lead to Dirac cones with massless Dirac fermions in *C2/m*, *Pbcm*, and *Pmmn* structures, while *Cmmm* structure exhibits Dirac ring feature (Figure 4a-d) [107]. Interestingly, BH sheets have been successfully prepared from MgB_2 by using cation-exchange method (Figure 4e-f) [108]. For Mg intercalation, the intercalated bilayer borophene (B_2MgB_2) can exhibit good phonon-mediated superconductivity with a high T_c of 23.2 K (Figure 4g-h) [102]. Moreover, a tensile strain in borophene is beneficial for superconducting [106]. Li doped borophene-graphene heterostructure shows gas-sensitive properties, which is promising for borophene-based gas sensors [109].

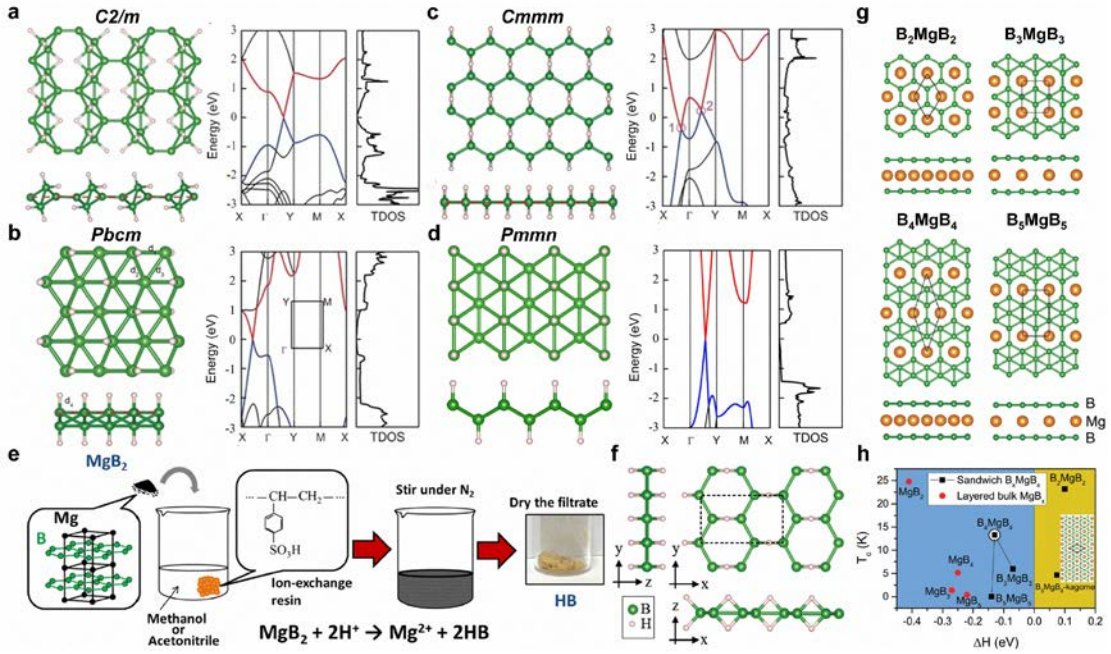

Figure 4. Surface modifications for borophene. (a-d) Top and side views as well as calculated band structures of (a) *C2/m*, (b) *Pbcm*, (c) *Cmmm*, and (d) *Pmmn* BH structures. (e) Synthesis process of BH sheets. (f) Proposed structure model of synthesized BH sheet. (g) Top and side views of 2D sandwich structures of B_2MgB_2, B_3MgB_3, B_4MgB_4, and B_5MgB_5. (h) Calculated T_c as a function of the formation enthalpy. (a-d) Reproduced with permission from ref. [107]. Copyright 2016 Wiley. (e, f) Reproduced with permission from ref. [108]. Copyright 2017 American Chemical Society. (g, h) Reproduced with permission from ref. [102]. Copyright 2017 Royal Society of Chemistry.

Gallenene and thallene. The surface modifications of aluminene and indiene have not been reported before, as the study on them is still in theoretical research stage without experimental realization. Therefore, this part will focus on gallenene and thallene. In 2018, few-layer gallenene was first obtained by solid melt exfoliation technique [29]. Thereafter, epitaxial growth method was used to prepare gallenene. The substrate and the loading amount of gallium can modify the atomic and electronic structures of gallenene. With a low loading amount of gallium, the monolayer gallenene grown on Si(111) displays a $4 \times \sqrt{13}$ superstructure (Figure 5a-d), while the second layer gallenene exhibits a hexagonal

Preprints (www.preprints.org) | NOT PEER-REVIEWED | Posted: 14 December 2022 doi:10.20944/preprints202212.0247.v1

honeycomb structure with a high loading amount (Figure 5e-f) [110]. The buckled honeycomb gallenene shows metallic properties (Figure 5g) [110]. Nevertheless, the growth behavior of gallenene on GaN(0001) substrate is totally different, showing a bilayer flat gallenene (Figure 5h-i) [111]. Excitingly, the bilayer hexagonal gallenene exhibits superconducting with a T_c of 5.4 K (Figure 5j-k) [111]. However, thallene has rarely been reported. Recently, honeycomb thallene has been successfully formed on $NiSi_2$/Si(111) substrate [112].

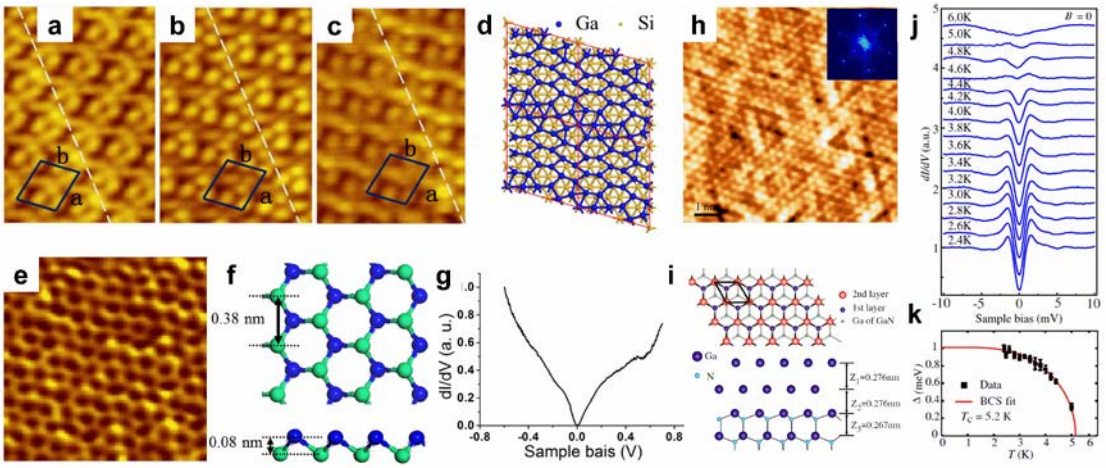

Figure 5. Surface modifications for gallenene. (a-c) STM images with the bias of 2.0, 1.6 and 1.0 V of monolayer gallenene on Si(111) substrate. (d) Proposed configuration of monolayer gallenene on Si(111). (e) STM image of the second layer gallenene on Si(111) substrate. (f) Top and side views of the proposed structure for the second layer gallenene. (g) *dI*/*dV* spectrum recorded on the second layer gallenene. (h) High-resolution STM image of gallenene on GaN(0001) substrate. (i) Top and side views of proposed gallenene structure on GaN(0001) substrate. (j) A series of *dI*/*dV* spectra recorded on gallenene/GaN at various temperatures. (k)Temperature-dependent superconducting gap magnitude and fitting to BCS gap function for gallenene/GaN. (a-g) Reproduced with permission from ref. [110]. Copyright 2018 IOP Publishing Ltd. (h-k) Reproduced with permission from ref. [111]. Copyright 2015 American Physical Society.

3.2. Group IV

Graphene. The sp^2 hybridization of carbon atoms leads to the formation of flat honeycomb graphene with a σ bond between neighboring carbon atoms [113]. The σ bond is the key for the high robustness of graphene with a Young's modulus of 1T Pa and a fracture strength of 130 GPa [114]. The unhybridized p orbit, perpendicular to the planar structure of graphene, binds covalently with neighboring carbon atoms to form a π band which is half-filled. Graphene is a semimetal, showing linearly dispersing bands near Fermi level with massless Dirac fermions [113]. As a result, graphene displays an ambipolar electric field effect and high carrier mobility [115]. In addition to its excellent transparent property, graphene becomes a low-cost alternative to indium tin oxides [116]. Furthermore, graphene exhibits impressive thermal properties with thermal conductivity ranging from 3000-5000 W m^{-1} K^{-1} [117].

Preprints (www.preprints.org) | NOT PEER-REVIEWED | Posted: 14 December 2022 doi:10.20944/preprints202212.0247.v1

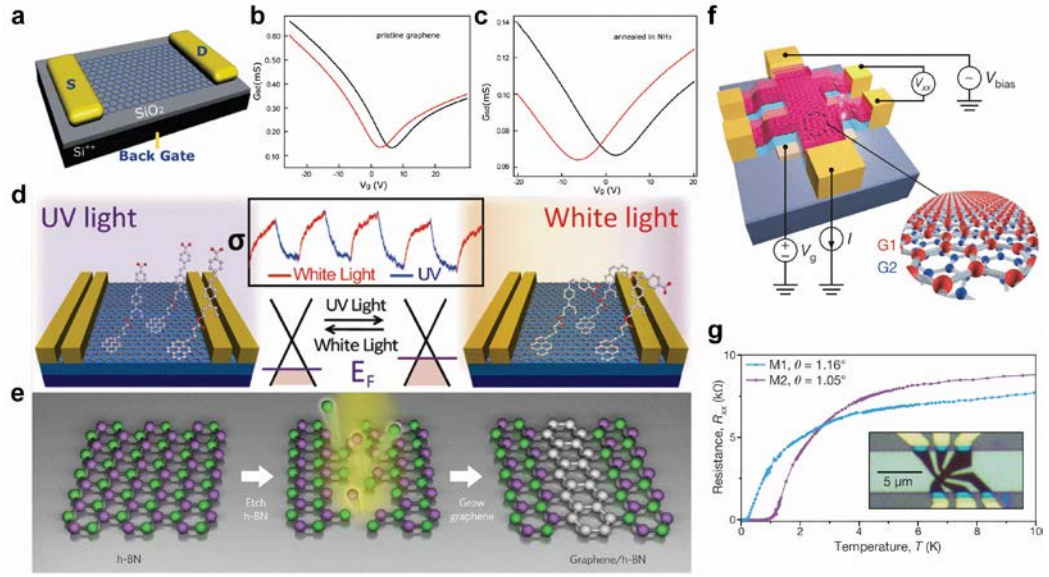

Figure 6. Surface modifications for graphene. (a-c) Comparison of the transfer characteristics of different graphene-based FET (black and red curves were measured in air and in vacuum respectively). (a) Scheme of the graphene-based FET device. (b, c) The transport properties of (b) pristine graphene and (c) graphene annealed in NH3 after irradiation measured at V_{sd} = 0.03 V. (d) Light-driven conductance modulation of graphene with adsorption of DR1P molecules. (e) Fabrication of in-plane graphene/h-BN heterostructures. (f) Schematic of a twisted bilayer graphene device and four-probe measurement system. (g) Superconductivity in twisted bilayer graphene. (a-c) Reproduced with permission from ref. [118]. Copyright 2010 American Chemical Society. (d) Reproduced with permission from ref. [36]. Copyright 2012 American Chemical Society. (e) Reproduced with permission from ref. [42]. Copyright 2013 Springer Nature Ltd. (f, g) Reproduced with permission from ref. [52]. Copyright 2018 Springer Nature Ltd.

Graphene's distinct physical characteristics make it potentially useful for field-effect transistors (FET), sensors, transparent conductive films, energy devices, etc., but its intrinsic gapless character still constrains its further applications. First, heteroatom doping or chemical adsorption can effectively tune the electronic properties of graphene. N doping can induce n-type doping (Figure 6a-c) [118] while B doping can introduce p-type transfer characteristics [119]. Chemical functional groups can also produce various doping effects. For example, the adsorption of spiropyran and DR1P molecules introduce n-type and p-type doping for graphene, respectively [36, 120]. Moreover, light can reversibly switch the molecular transformations, resulting in the controllable shift of Dirac point of graphene(Figure 6d) [36, 120]. By seamlessly and precisely stitching the domains of graphene and h-BN (Figure 6e), the hybrid atomic layers of in-plane heterostructures can be applied for intriguing electronic applications [42, 121]. Inconceivably, for the proper twisted angles of bilayer graphene, the electronic band structure shows flat bands near Fermi energy, resulting in the correlated insulating states at half-filling and unconventional superconductivity with T_c of 1.7 K (Figure 6f-g) [52].

Silicene. Silicene, the silicon analog of graphene, was first predicted in a theoretical study [122] and first realized experimentally by epitaxial growth on Ag(110) [20]. Unlike that the sp^2 hybridization of carbon atoms induces a flat honeycomb structure of graphene, silicon prefers the mixed sp^2-sp^3 hybridization to form a low-buckled honeycomb silicene, retaining the existence of Dirac fermions [123, 124]. Considering spin-orbit coupling (SOC) effect, silicene is predicted to have a spin-orbit gap of 1.55 meV, much larger than that of graphene [16]. Owing to its topologically nontrivial electronic structures, silicene exhibits many unique physical properties, including quantum spin Hall (QSH) effect [16, 125], giant magnetoresistance [126, 127], field-tunable bandgap [128, 129], and nonlinear electro-optic effects [130]. Hence, silicene shows great potential for device applica-

Preprints (www.preprints.org) | NOT PEER-REVIEWED | Posted: 14 December 2022 doi:10.20944/preprints202212.0247.v1

tions, especially for gate-controlled topological FET [131]. Although silicene has been prepared on many substrates, the poor air stability of silicene is the major challenge, requiring proper encapsulation or passivation of reactive surface for device fabrication [132, 133].

Due to the limitations from poor air-stability of silicene, it is difficult to experimentally perform surface modifications for silicene. Theoretical investigations on the surface modifications of silicenen focus on doping, strain, hydrogenation, intercalation, and chemical adsorption. Transition metal adsorption can induce various doping effect for silicene (n-type by Cu, Ag and Au adsorption, p-type by Ir adsorption, and neutral type by Pt adsorption in Figure 7a) [134], and so can applying strain [135]. Moreover, Mn doping can induce a ferromagnetic state for silicene, which can be transformed to an antiferromagnetic state with the application of biaxial strain (Figure 7b) [136]. Under certain pressure strain, the spin-orbit bandgap of silicene will increase from 1.55 to 2.9 meV [16]. One-side semi-hydrogenation can introduce ferromagnetism to silicene, as well as make it semiconducting with a direct bandgap of 1.74 eV (Figure 7c-d) [137]. Oxygen intercalation into the underlying silicene on Ag(111) surface can effectively reduce the orbital hybridization of the top-layer silicene and Ag substrate, leading to massless Dirac fermions (Figure 7e-g) [138]. However, in K-intercalated bilayer silicene, the Dirac cones are recovered with a small bandgap of 0.27 eV [139]. Chemical adsorption (gas and organic molecules) can tune the electronic properties of silicene, which could be a better candidate to detect gas and organic molecules compared to graphene [109, 140, 141].

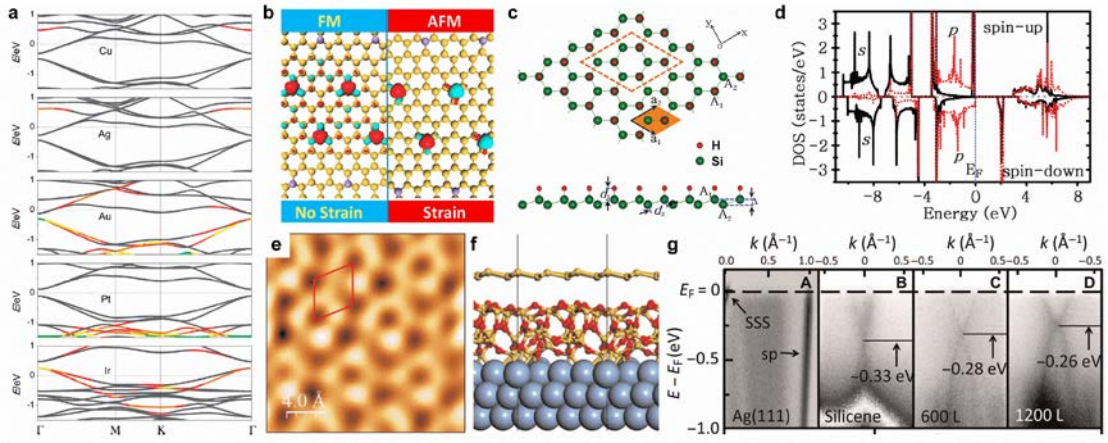

Figure 7. Surface modifications for silicene. (a) Electronic band structures of Cu, Ag, Au, Pt, and Ir-covered silicene at the coverage of 5.6%. The Fermi level is set to zero. (b) Strain controlled magnetic exchange coupling in Mn-doped silicene. (c) Top and side views of the atomic structure for one-side semi-hydrogenated silicene. (d) Partial density of states calculated by HSE06 for semi-hydrogenated silicene. (e) High resolution STM image of oxygen-intercalated epitaxial silicene grown on Ag(111). (f) Atomic structure of silicene/SiO_x/Ag(111) from ab initio molecular dynamics (AIMD) simulation. (g) Energy versus k dispersion measured by ARPES for clean Ag(111) surface (A), as-grown $\sqrt{3} \times \sqrt{3}$ silicene formed on buffer layer (B), oxygen-intercalated silicene with an oxygen dose of 600 L (C), and intercalated silicene with an oxygen dose of 1200 L (D). (a) Reproduced with permission from ref. [134]. Copyright 2014 Royal Society of Chemistry. (b) Reproduced with permission from ref. [136]. Copyright 2017 American Chemical Society. (c, d) Reproduced with permission from ref. [137]. Copyright 2012 Royal Society of Chemistry. (e-g) Reproduced with permission from ref. [138]. Copyright 2016 American Association for the Advancement of Science.

Germanene. Germanene, similar to silicene, shows a low-buckled honeycomb structure, leading to the topologically nontrivial electronic structure with a spin-orbit bandgap of 23.9 meV due to its greater SOC than that of graphene and silicene [16, 142, 143]. These characteristics make germanene a promising candidate for applications in high-speed and low-energy-consumption devices since it has a high charge carrier mobility and exhibits QSHE [143]. Germanene has also been successfully prepared by epitaxial growth on various substrates.

Preprints (www.preprints.org) | NOT PEER-REVIEWED | Posted: 14 December 2022 doi:10.20944/preprints202212.0247.v1

Doping various atoms can introduce totally different influences on the physical properties of germanene. For instance, the adsorption of alkali metal atoms makes the semimetallic germanene become metallic with Dirac point moving below Fermi level and an opened small bandgap at Dirac point, while the adsorption of halogen atoms could lead to relatively large bandgaps ranging from 0.416 to 1.596 eV, promising for optoelectronic applications [144-146]. The adsorption of transition metal atoms (e.g., Ti, Sc, V, Cr, Mn, Fe, and Co) can induce magnetism, while nonmagnetic semiconducting states are realized for Ni, Cu, and Zn adsorption [147, 148]. The atomic structures of germanene can be controlled by the supported substrate and growth conditions. Directly grown on Ag(111) surface, two distinct phases of germanene can be observed: One shows striped phase, a honeycomb lattice partially commensurate with the substrate; the other is a quasi-freestanding phase, a honeycomb lattice incommensurate with the substrate [149]. By epitaxially prepared on Ag(111) thin film grown on Ge(111) with a segregation method, the germanene shows a highly ordered long-range superstructure with two types of protrusions (hexagon and line), resulting in a $(7\sqrt{7} \times 7\sqrt{7})R19.1^{o}$ supercell with respect to Ag(111) (Figure 8a-b) [150]. However, the single domain (3 × 3) and multi domain $(\sqrt{7} \times \sqrt{7})R(\pm 19.1^{o})$ of germanene can exist simultaneously on Al(111) surface (Figure 8c) [151]. On MoS_2 substrate, germanene islands can be formed at high deposition rates, whereas Ge atoms prefer to intercalate between MoS_2 layers to form Ge clusters at low deposition rates [146, 152]. On Au(111) surface, the honeycomb (1 × 1) germanene with buckled structure has been identified in a $(\sqrt{7} \times \sqrt{7})$ superstructure, exhibiting distinctive vibrational phonon modes, enhancing electron-phonon coupling induced by the tensile strain [153].

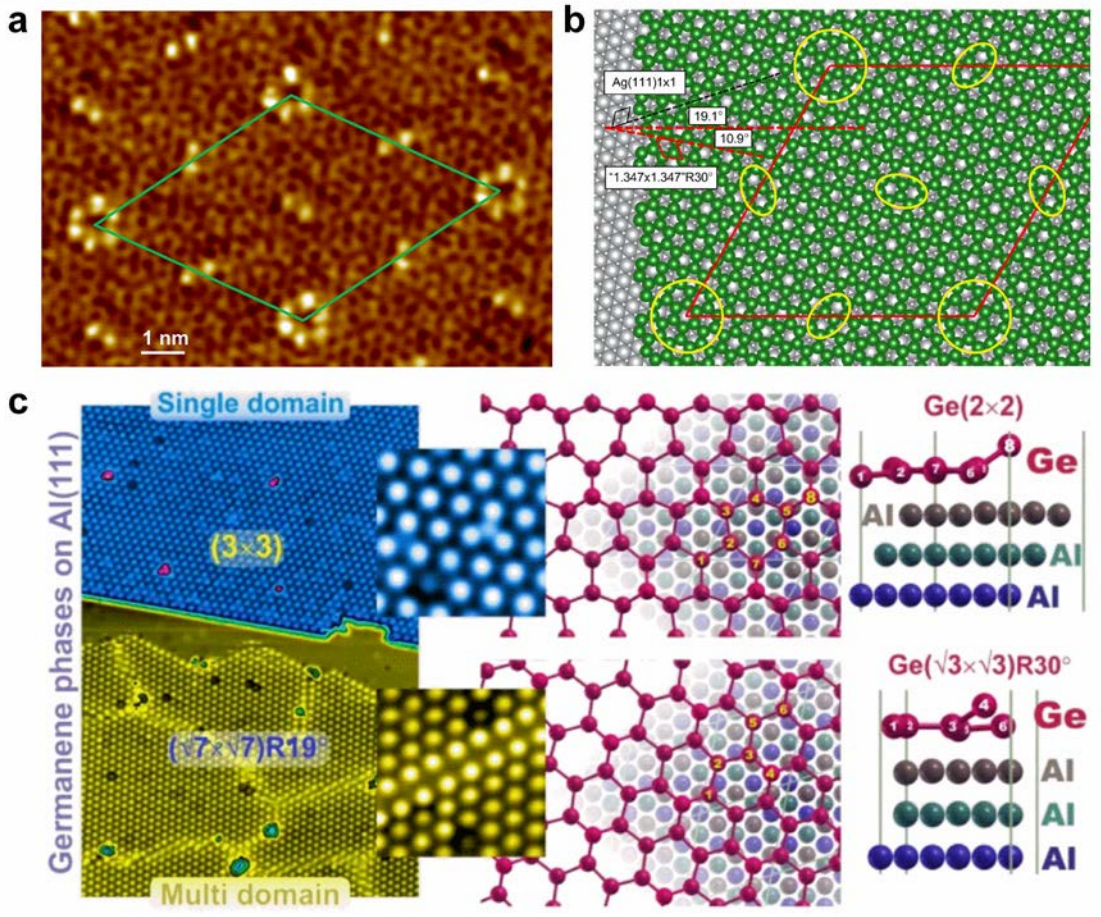

Figure 8. Surface modifications of germanene. (a) Atomic-scale STM image of germanene grown on a Ag(111) thin film. (b) Structural model of germanene on Ag(111). (c) Two different phases of germanene grown on Al(111) surface. (a, b) Reproduced with permission from ref. [150]. Copyright

Preprints (www.preprints.org) | NOT PEER-REVIEWED | Posted: 14 December 2022 doi:10.20944/preprints202212.0247.v1

2018 American Chemical Society. (c) Reproduced with permission from ref. [151]. Copyright 2019 Springer Nature Ltd.

Stanene. Analogously, monolayer Sn prefers to form a low-buckled structure due to the mixed sp^2-sp^3 hybridization of Sn atoms [154]. Stanene has been predicted to have massless Dirac fermions and open a spin-obit bandgap of 0.1 eV at the K point with SOC [154]. The bandgap at Dirac point can produce a conductive 1D helical edge state with opposite spin polarization, allowing for the low-power spintronic applications [13, 155].

The double-side decorated stanene by chemical functional groups appears in the most stable configuration (Figure 9a). For prinstine stanene, SOC can open a bandgap of 0.1 eV at the K point, thus stanene becomes a QSH insulator (Figure 9c). After hydorgenation or fluorination, the bandgap at the K point is substantially enlarged because of the saturation of the π orbital (Figure 9d-e). Fluorination induces a parity exchange between occupied and unoccupied bands at the Γ point. In details, a negative-parity Blaoch state shifts downwards into valence bands, leaving a positive-parity Bloch state as the conduction band minimum (Figure 9d), leading to a topologically nontrivial band structure. Nonetheless, the band inversion at Γ point cannot be seen for hydrogenated stanene (Figure 9e). In fact, the band inversion exists for several chemical functional groups (Halogen atoms and -OH) (Figure 9b).

Stanene is predicted to show superior sensing performance for small molecules. CO, O_2, NO, NO_2 and SO_2 molecules act as charge acceptors, whereas H_2O, NH_3, and H_2S molecules act as charge donors [156, 157]. In addition, molecules' adsorption can effectively tune the work function of stanene (Figure 9f) [156]. The edge shapes of stanene play a key role in the physical properties of stanene nanoribbons (NRs). The armchair stanene NRs are nonmagnetic semiconductors with tunable bandgaps by ribbon width, whereas the zigzag stanene NRs present antiferromagnetic ground states with opposite spin order between the two edges [158]. Generally, the energy gap (0.1 eV) of monolayer stanene rules out the phonon-meidated superconductivity. Interestingly, doping with Ca (Li) can lead to superconductivity with a low Tc of ~1.3 K (~1.4 K), lower than the value (3.7 K) of bulk β-tin [159].

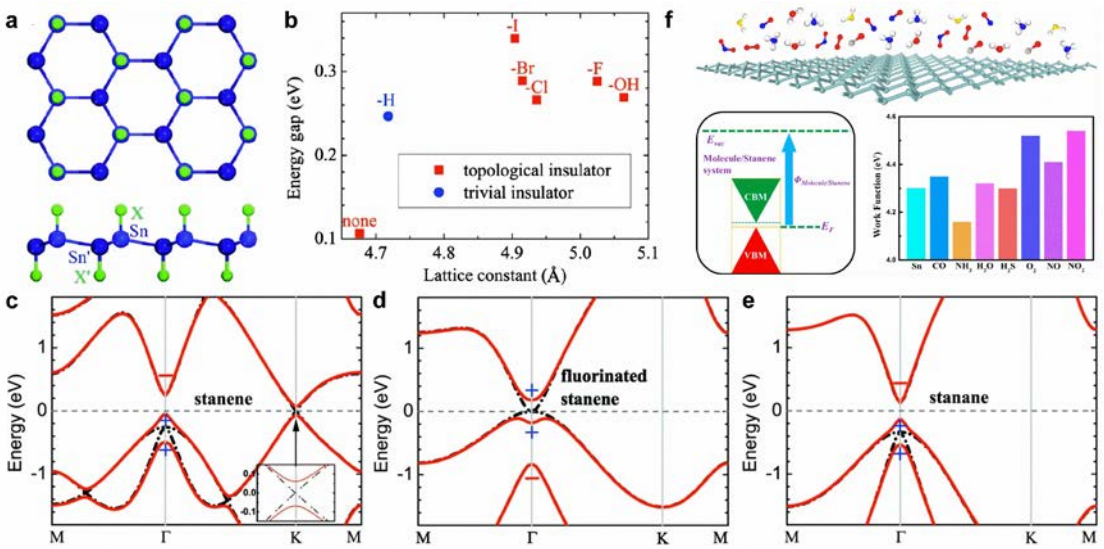

Figure 9. Surface modifications for stanene. (a) Crystal structure for decorated stanene by hydrogen or halogen atoms from both sides. (b) The calculated energy gap for stanene and decorated stanene. (c-e) Band structures for (c) stanene, (d) fluorinated stanene, and (e) stanine without (black dash-dotted lines) and with (red solid lines) SOC. Parities of the Bloch states at the Γ point are denoted by +, -. (f) Structural model of stanene for adsorption of various molecules and work function of stanene with various adsorbed molecules. (a-e) Reproduced with permission from ref. [154]. Copyright 2013 American Physical Society. (f) Reproduced with permission from ref. [156]. Copyright 2016 American Chemical Society.

Preprints (www.preprints.org) | NOT PEER-REVIEWED | Posted: 14 December 2022 doi:10.20944/preprints202212.0247.v1

Plumbene. Unlike other four Xenes in main group IV, no Dirac point crosses linearly from Pb p_z orbit at the K point without SOC. Although turning on SOC opens a large bandgap of ~400 meV, no Dirac edge state is observed in the bandgap of plumbene [160]. In addition, resulting from the energy decrease of s antibonding state from graphene to plumbene, the s antibonding state is lower than all p bonding and antibonding states at the Γ point in plumbene, totally different from graphene, silicene, germanene, and stanene [161]. Therefore, plumbene is a normal insulator with a topologically trivial character. However, through electron doping, plumbene can become a topological insulator with a large bulk gap (~200 meV) [162]. Decorated plumbene by chemical function groups (hydrogen and halogen atoms) can transform from a normal insulator to a QSH insulator with giant bulk gaps from 1.03 to 1.34 eV [160]. Plumbene has been predicted to be magnetic with Ti, V, Cr, Mn, Fe, and Co doping, while Sc and Ni doped plumbene is nonmagnetic [163]. It is interesting that plumbene can be successfully grown by segregation on a $Pd_{1-x}Pb_x(111)$ alloy surface [30]. Furthermore, a c(2 × 4) structure of Pb is formed on Ir(111) substrate, whereas a flat honeycomb plumbene can be formed on an Fe monolayer on Ir(111) [164].

3.3. Group V

Phosphorene. The puckered and buckled phosphorene are the most common allotropic monolayer structures, corresponding to the individual atomic layer of black phosphorous and blue phosphorous crystals respectively [165]. Puckered monolayer phosphorene is semiconducting with a direct bandgap of 1.83 eV whereas buckled monolayer phosphorene is a semiconductor with an indirect bandgap of 2.0 eV. Phosphorene can be obtained through mechanical exfoliation, liquid phase exfoliation, electrochemical exfoliation, chemical vapor deposition, epitaxial growth, etc [165]. To date, semiconducting character of phosphorene leads to some experimental demonstration in various applications, including electronics, optoelectronics, photovoltaics, supercapacitors, and catalysis [73, 166].

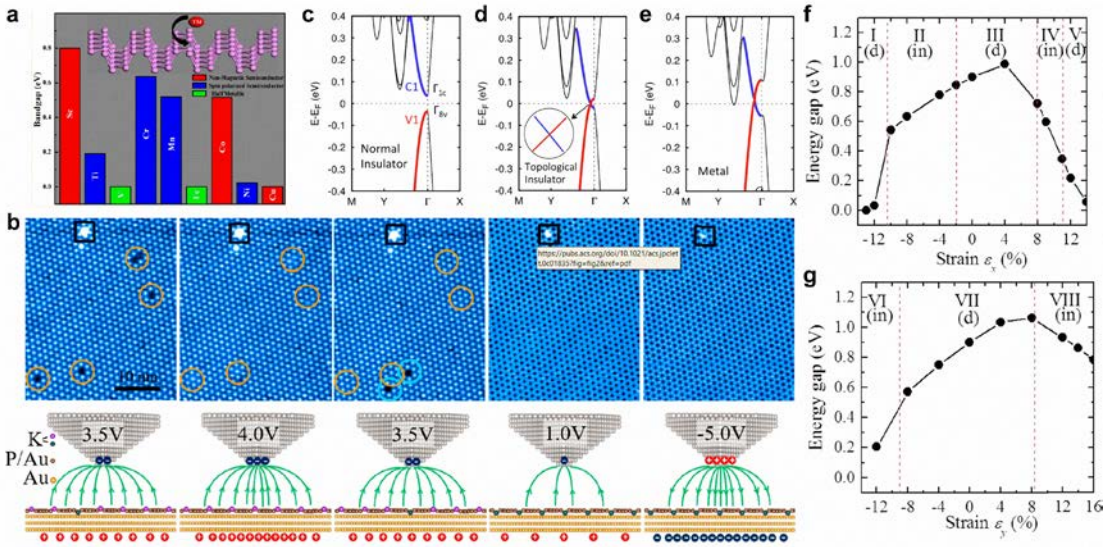

Figure 10. Surface modifications for phosphorene. (a) Electronic and magnetic properties of transition metal doped phosphorene. (b) STM images of blue phosphorene-Au network with 1ML K deposition scanned with different bias voltages. (c-e) Band structures of 4-layer phosphorene with an external electric field of (c) 0 V $Å^{-1}$, (d) 0.45 V $Å^{-1}$, and (e) 0.6 V $Å^{-1}$. (f, g) Bandgap of phosphorene as a function of strain (f) ε_x applied in the zigzag and (g) ε_y in the armchair directions. (a) Reproduced with permission from ref. [167]. Copyright 2015 American Chemical Society. (b) Reproduced with permission from ref. [168]. Copyright 2020 American Chemical Society. (c-e) Reproduced with permission from ref. [169]. Copyright 2015 American Chemical Society. (f, g) Reproduced with permission from ref. [51]. Copyright 2014 American Physical Society.

 doi:10.20944/preprints202212.0247.v1

The transition metal doped black phosphorene possesses dilute magnetic semiconducting properties. In particular, substitutional doping of Ti, Cr, and Mn can create a spin-polarized semiconducting state, while a half-metallic state is realized by V and Fe doping (Figure 10a) [167]. Both Fe-doping and N-doping can significantly improve the electrocatalytic activity of black phosphorene for nitrogen reduction reaction [170, 171]. For blue phosphorene, B-doping and C-doping can both improve the sensitivity of NH_3 gas molecules, and the sensitivity of CO gas molecules can be enhanced by B-doping [172]. With monotonic increase of an external electric field, black phosphorene can transit from the normal insulator to a topological insulator and eventually to a metal (Figure 10c-e) [169]. In addition, an external electric field can realize reversible potassium intercalation in the blue phosphorene-Au network (Figure 10b) [168]. When axial strain is applied in the zigzag or armchair direction, the bandgap of black phosphorene will exhibit a direct-indirect-direct transition (Figure 10f-g) [51]. Moreover, a topological phase transition of black phosphorene can be realized by the application of compressive biaxial in-plane strain and perpendicular tensile strain [173].

Arsenene. Arsenene mainly has two kinds of allotropic structures, including buckled and puckered [165]. Buckled honeycomb monolayer arsenene, derived from semimetallic gray arsenic, shows an indirect bandgap of 2.49 eV [24], while puckered monolayer arsenene, exfoliated from black semiconducting arsenic, possesses an indirect bandgap of 0.831 eV [75]. Both buckled and puckered arsenene has thickness-dependent bandgaps. The methods to obtain arsenene include up-down (mechanical exfoliation and liquid phase exfoliation), and bottom-up strategies (molecular beam epitaxy, chemical vapor deposition, physical vapor deposition, etc.) [174]. For epitaxial growth, monolayer buckled arsenene has been successfully grown on Ag(111) substrate [175], whereas monolayer armchair arsenene nanochains are formed on Au(111) surface [32]. 2D arsenene has been theoretically predicted to exhibit various physical properties, such as indirect-to-direct bandgap transition, semimetal-to-semiconductor transition, superconductivity, and QSH effect, deserving many research efforts [24, 176, 177]. Recently, few-layer black arsenene is proved to exhibit the particle-hole asymmetric Rashba valley and exotic quantum Hall states due to the synergetic effects between spin-orbit interaction and the Stark effect [178].

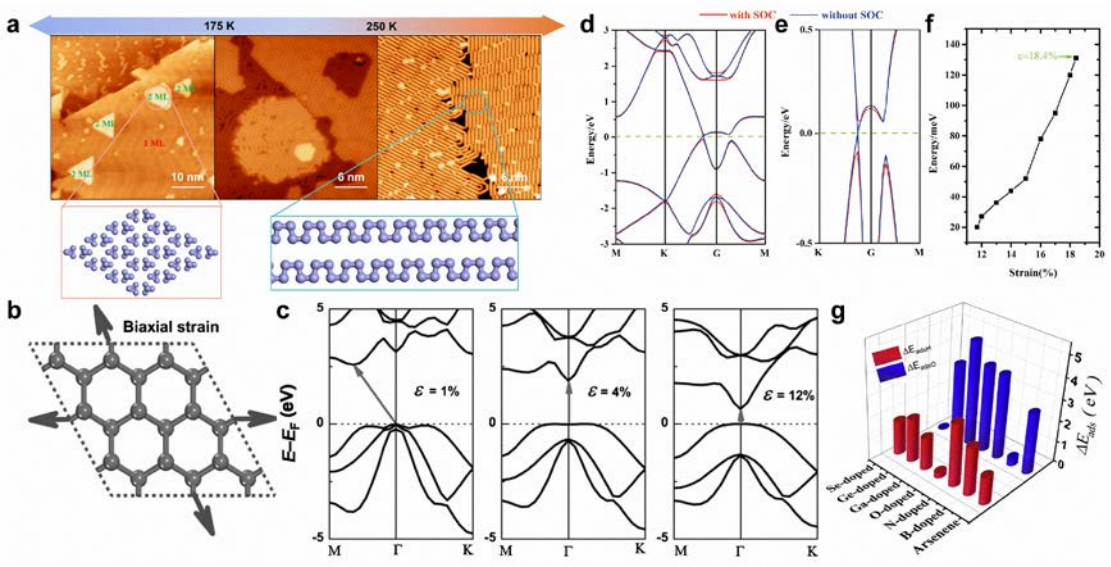

Figure 11. Surface modifications for arsenene. (a)Schematic diagram of substrate-temperature-dependent arsenic nanostructures on Au(111) substrate. (b) Schematic representation of arsenene under biaxial tensile strain. (c) Variation of electronic band structures of arsenene under various biaxial strain. (d, e) Band structure of arsenene under the biaxial tensile strain of 18.4% and the enlarged view. (f) Bandgap variation of arsenene with the tensile strain. (g) Adsorption energy of hydrogen and oxygen on pristine and B, N, O, Ga, Ge, and Se doped arsenene. (a) Reproduced with permission from ref. [32]. Copyright 2022 American Chemical Society. (b, c) Reproduced with permission from

 doi:10.20944/preprints202212.0247.v1

ref. [24]. Copyright 2015 Wiley. (d-f) Reproduced with permission from ref. [176]. Copyright 2015 Royal Society of Chemistry. (g) Reproduced with permission from ref. [179]. Copyright 2018 Elsevier Ltd.

Substrate temperature can modify the formation of arsenic nanostructures. On Au(111) substrate, the arsenic monolayer formed by 0D tetrahedral As_4 clusters can transform to monolayer formed by 1D armchair arsenene nanochains (Figure 11a) [32]. The application of biaxial tensile strain can effectively tune the band structures of arsenene. Under small tensile strain, arsenene can be transform from indirect to direct bandgap (Figure 11b-c) [24]. With further enlarging the tensile strain, the direct bandgap will gradually disappear, causing band inversion at the Γ point (Figure 11d-e) [176]. The consideration of SOC can open a spin-orbit bandgap (~131 meV) under the tensile strain of 18.4% (Figure 11f), indicating QSH effect in arsenene [176]. Intriguingly, under proper biaxial tensile strain and electron doping, arsenene can be superconducting with T_c of 30.8 K [177]. Certainly, 3d transition metal doping can strongly tailor the electronic and magnetic properties of arsenene. Ti, V, Cr, Mn, and Fe doping can induce magnetic states for arsenene [180]. Meanwhile, Ti and Mn doping leads to a half-metallic state, while V, Cr, and Fe doping results in a spin-polarized semiconducting state [180]. In addition, doping can further modify the chemical properties, making arsenene potential for hydrogen evolution reaction and oxygen evolution reaction (Figure 11g) [179].

Antimonene and Bismuthene. The most stable structures of antimonene and bismuthene are α-form (puckered) and β-form (buckled), which are the monolayers of black and grey bulk allotropes respectively. Monolayer β-Sb and β-Bi possess indirect bandgaps of 2.28 and 0.99 eV respectively, whereas the direct bandgaps of monolayer α-Sb and α-Bi are 1.18 and 0.36 eV respectively [74, 181, 182]. Notably, the calculated bandgaps may vary depending on the used methods. Both antimonene and bismuthene exhibit tunable bandgap, high carrier mobility, high stability, and in-plane anisotropy, providing the ground for multifunctional applications in electronics, optoelectronics, sensors, batteries, etc. [183-185].

Doping with 3d transition metal atoms for antimonene can lead to significant changes in bandgap and magnetic moment [186]. For Cr-doped β-antimonene, a spin-polarized semiconducting state was predicted. For Ti-, Mn-, and V-doped β-antimonene, half-metallic behavior has been calculated. Similarly, Cr-doped bismuthene structure leads to a spin-polarized semiconducting state, while V-doped bismuthene can produce magnetic metal character and the Mn and Fe replacing systems result in half-metal features [187]. Additionally, V-doped systems exhibit ferromagnetism (FM) when two V atoms are far apart, but Cr-, Mn-, and Fe-doped bismuthene exhibit anti-ferromagnetism (AFM) when two impurity atoms are close together or far apart [187]. Bivacancies doping in β-antimonene can reduce the bandgap of pristine β-antimonene, but monovacancy doped β-antimonene exhibits a metallic character [188]. Electron-doping and Ca-intercalation can transform bilayer β-antimonene from a semimetal to a superconductor [189]. Moreover, the physisorption of organic molecules (tetrathiafulvalene and tetracyanoquinodimethane) can induce n-type and p-type doping for antimonene, respectively [190]. Under monotonic increase of biaxial tensile strain, β-antimonene and β-bismuthene undergo the transition of indirect-to-direct bandgap and semiconducting to semimetallic, and even topological phase transition [24, 191, 192].

3.4. Group VI

Selenene and Tellurene. Selenene has been predicted to have 3 allotropic structures, including 1T-MoS_2-like structure (t-Se or α-Se), tiled helical-chain structure (c-Se), and square structure (s-Se) [193]. Both t-Se and c-Se are semiconductors with indirect bandgaps of 0.71 and 1.74 eV respectively, while s-Se is semimetallic. The formation energy of c-Se is the lowest, indicating that c-Se is the most stable phase. In addition, a ring structure of selenene (r-Se) is proposed [58]. However, theoretical investigations predict

Preprints (www.preprints.org) | NOT PEER-REVIEWED | Posted: 14 December 2022 doi:10.20944/preprints202212.0247.v1

the existence of 3 phases of tellurene, including α-, β-, and γ-phases, possessing 1T-MoS_2-like, rectangle, and 2H-MoS_2-like structures respectively [27]. It is found that α- and β-Te show semiconducting character with indirect bandgaps of 0.76 and 1.17 eV, respectively, whereas γ-Te is a metal. It is interesting that the band structures of square selenene and tellurene (s-Se and s-Te) show Dirac-cone-like dispersions. A large bandgap (~0.1 eV) opened by SOC makes them become topological insulators and host non-trivial edge states [58]. Therefore, square selenene and tellurene become promising candidates for spintronic applications. The tensile strain can monotonically decrease the bandgaps of α-Se and α-Te [194, 195]. Meanwhile, for 2D square tellurene under strain effect, the system displays three structural phases: buckled square, buckled rectangle, and planar square phases, exhibiting extraordinary topological properties [195]. In particular, the buckled rectangle tellurene can act as a QSH insulator with a bandgap of 0.24 eV.

4. Applications of 2D Xenens

As mentioned above, 2D Xenes possess various physical and chemical properties, such as flexibility, layer-dependent semiconductor, high carrier mobility, sensitivity of molecules and light, topologically nontrivial band structures, etc.

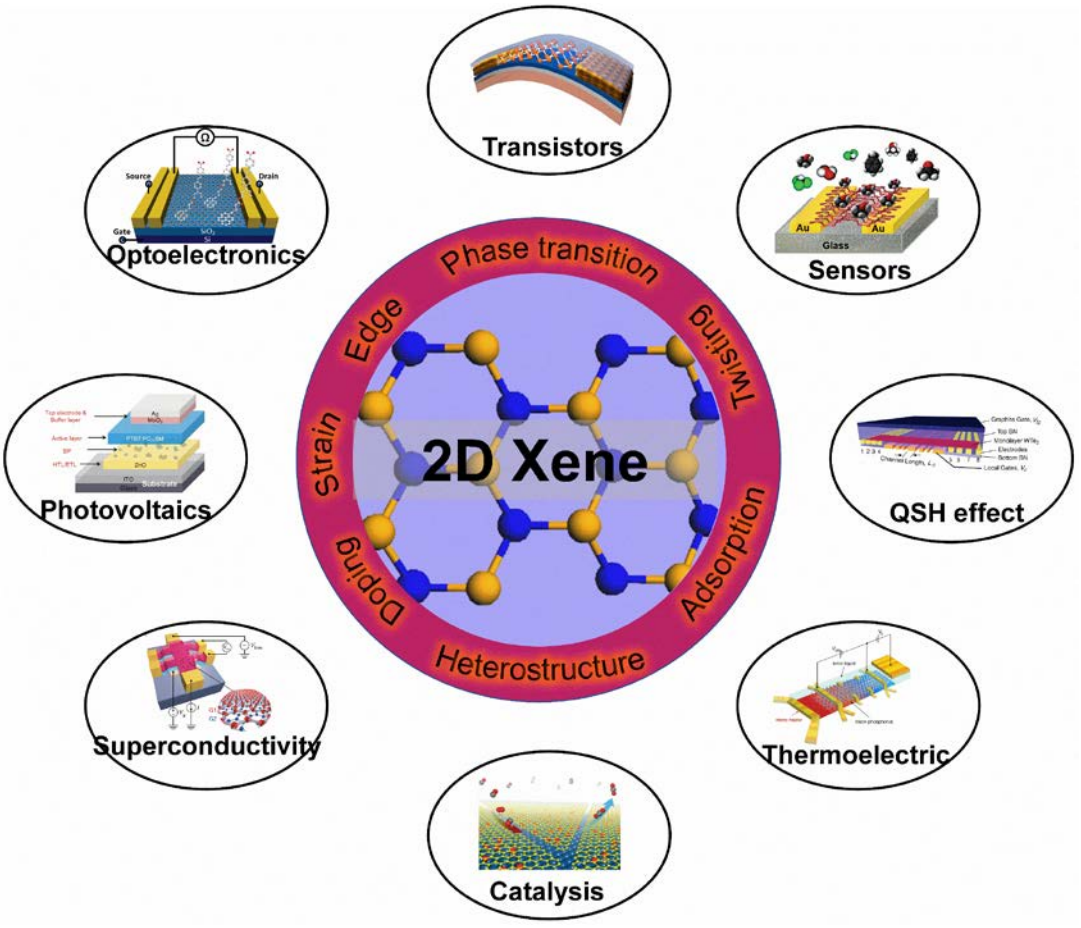

Figure 12. Applications of 2D Xenens with surface modifications. Transistors: Reproduce with permission from ref. [196]. Copyright 2015 American Chemical Society. Optoelectronics: Reproduce with permission from ref. [36]. Copyright 2012 American Chemical Society. Sensors: Reproduce with permission from ref. [197]. Copyright 2015 American Chemical Society. Photovoltaics: Reproduce with permission from ref. [198]. Copyright 2016 Wiley. QSH effect: Reproduce with permission from ref. [199]. Copyright 2018 American Association for the Advancement of Science. Superconductivity: Reproduce with permission from ref. [52]. Copyright 2018 Springer Nature Ltd. Thermoelectric: Reproduce with permission from ref. [200]. Copyright 2016 American Chemical Society. Catalysis: Reproduce with permission from ref. [201]. Copyright 2014 National Academy of Science.

 doi:10.20944/preprints202212.0247.v1

In order to utilize 2D Xenes more effectively, surface modifications become particularly important (Figure 12) to tune the properties of 2D Xenes. For instance, the FET of acene-type graphene nanoribbons exhibits excellent semiconductor characteristics with on/off ratio of 88 [202]. To enhance the mid-infrared (MIR) absorption of graphene, the localized surface plasmon resonance of B-doped Si quantum dots (QDs) result in the QD/graphene hybrid photodetector with ultrahigh responsivity, gain, and specific detectivity in the UV-to-MIR region [34]. Solution exfoliated black phosphorene flakes as electron transport layer can enhance the performance of organic solar cells [198]. In addition, layered black phosphorene exhibits a selective detection for methanol [197]. Graphene/Pt(111) surface can occur surface reactions of CO adsorption/desorption and CO oxidation [201]. Overall, thanks to surface modifications, 2D Xenes show great potential for applications in plenty of fields.

5. Conclusions

Totally, except graphene, 15 different elemental 2D materials of main group elements have been experimentally realized or theoretically predicted to date. In fact, 14 Xenes, including borophene, graphene, silicene, phosphorene, gallenene, germanene, arsenene, selenene, stanene, antimonene, tellurene, thallene, plumbene, and bismuthene, have been successfully grown on proper substrates by epitaxial methods. Although a lot of research, engineering, and development about 2D Xenes, most of which are investigated theoretically, have been reported in recent years, experimental studies are still desperately required for the development of synthesis strategies and novel applications. Before realizing the surface modifications of 2D Xenes for the applications of interest, three significant challenges need to be overcome:

(i) The synthesis strategies of 2D Xenes must not only ensure reliably large-scale production, but also be tailored for the requirements of application. For example, the applications of electronics and batteries demand low cost and scalable techniques, while plasmonics and spintronics require high fidelity and reproducible techniques. Hence, the reliable synthesis approaches play a crucial role in functional design and practical applications.

(ii) The strategies to enhance the environmental stability and to mitigate the degradation of 2D Xenes must be taken into consideration for the particular applications. For instance, the optoelectronic device based on black phosphorene must be concerned with ambient stability, requiring appropriate encapsulation or passivation of the surface.

(iii) Many of the just-predicted fascinating properties of 2D Xenes require further efforts to explore strategies for their implementation, which may offer opportunities to discover revolutionary technologies. In addition, the exciting and novel properties necessitate not just "one-off" research, but also statistical evaluation to ascertain their viability and accessibility on a commercial scale.

Despite the facing challenges ahead, the exceptional properties of 2D Xenes will significantly impact the future applications in various fields. It is hoped that this review will inspire more exhilarating discoveries and applications in the growing family of 2D Xenes.

Author Contributions: Conceptualization, Y.M.; validation, J.C., C.W., X.X., W.Z. and Y.M.; investigation, J.C., C.W., H.L., X.X., J.Y., Z.H., L.W. and Y.M.; resources, J.C., C.W. and Y.M.; data curation, J.C., C.W. and Y.M.; writing—original draft preparation, J.C., C.W., and Y.M.; writing—review and editing, X.X., W.Z. and Y.M.; visualization, Y.M.; project administration, Y.M.; funding acquisition, Y.M. J.C. and C.W. contributed equally to this work. All authors have read and agreed to the published version of the manuscript.

Funding: This work is financially supported by the Start-up Foundation of Henan University (Grant No.: CX3050A0970531).

Institutional Review Board Statement: Not applicable.

Informed Consent Statement: Not applicable.

Data Availability Statement: Data is contained within the article.

Acknowledgments: We thank Dr. J. Li for helpful discussions.

Conflicts of Interest: The authors declare no conflict of interest.

References

1. Novoselov, K. S.; Geim, A. K.; Morozov, S. V.; Jiang, D.-e.; Zhang, Y.; Dubonos, S. V.; Grigorieva, I. V.; Firsov, A. A., Electric field effect in atomically thin carbon films. *Science* **2004,** 306, 5696, 666-669.
2. Mannix, A. J.; Kiraly, B.; Hersam, M. C.; Guisinger, N. P., Synthesis and chemistry of elemental 2D materials. *Nat. Rev. Chem.* **2017,** 1, 2, 1-14.
3. Kis, A., Graphene is not alone. *Nat. Nanotechnol* **2012,** 7, 683.
4. Butler, S. Z.; Hollen, S. M.; Cao, L.; Cui, Y.; Gupta, J. A.; Gutiérrez, H. R.; Heinz, T. F.; Hong, S. S.; Huang, J.; Ismach, A. F., Progress, challenges, and opportunities in two-dimensional materials beyond graphene. *ACS Nano* **2013,** 7, 4, 2898-2926.
5. Xiao, X.; Song, H.; Lin, S.; Zhou, Y.; Zhan, X.; Hu, Z.; Zhang, Q.; Sun, J.; Yang, B.; Li, T., Scalable salt-templated synthesis of two-dimensional transition metal oxides. *Nat. Commun.* **2016,** 7, 1, 1-8.
6. Huang, B.; Clark, G.; Navarro-Moratalla, E.; Klein, D. R.; Cheng, R.; Seyler, K. L.; Zhong, D.; Schmidgall, E.; McGuire, M. A.; Cobden, D. H., Layer-dependent ferromagnetism in a van der Waals crystal down to the monolayer limit. *Nature* **2017,** 546, 7657, 270-273.
7. Burch, K. S.; Mandrus, D.; Park, J.-G., Magnetism in two-dimensional van der Waals materials. *Nature* **2018,** 563, 7729, 47-52.
8. Zhang, Y.-Z.; El-Demellawi, J. K.; Jiang, Q.; Ge, G.; Liang, H.; Lee, K.; Dong, X.; Alshareef, H. N., MXene hydrogels: fundamentals and applications. *Chem. Soc. Rev.* **2020,** 49, 20, 7229-7251.
9. Zhang, C. J.; McKeon, L.; Kremer, M. P.; Park, S.-H.; Ronan, O.; Seral-Ascaso, A.; Barwich, S.; Coileáin, C. Ó.; McEvoy, N.; Nerl, H. C., Additive-free MXene inks and direct printing of micro-supercapacitors. *Nat. Commun.* **2019,** 10, 1, 1-9.
10. Novoselov, K.; Mishchenko, o. A.; Carvalho, o. A.; Castro Neto, A., 2D materials and van der Waals heterostructures. *Science* **2016,** 353, 6298, aac9439.
11. Li, L.; Kim, J.; Jin, C.; Ye, G. J.; Qiu, D. Y.; Da Jornada, F. H.; Shi, Z.; Chen, L.; Zhang, Z.; Yang, F., Direct observation of the layer-dependent electronic structure in phosphorene. *Nat. Nanotechnol.* **2017,** 12, 1, 21-25.
12. Ma, Y.; Shao, X.; Li, J.; Dong, B.; Hu, Z.; Zhou, Q.; Xu, H.; Zhao, X.; Fang, H.; Li, X., Electrochemically exfoliated platinum dichalcogenide atomic layers for high-performance air-stable infrared photodetectors. *ACS Appl. Mater. Inter.* **2021,** 13, 7, 8518-8527.
13. Hasan, M. Z.; Kane, C. L., Colloquium: topological insulators. *Rev. Mod. Phys.* **2010,** 82, 4, 3045.
14. Konig, M.; Wiedmann, S.; Brune, C.; Roth, A.; Buhmann, H.; Molenkamp, L. W.; Qi, X.-L.; Zhang, S.-C., Quantum spin Hall insulator state in HgTe quantum wells. *Science* **2007,** 318, 5851, 766-770.
15. Kane, C. L.; Mele, E. J., Quantum spin Hall effect in graphene. *Phys. Rev. Lett.* **2005,** 95, 22, 226801.
16. Liu, C.-C.; Feng, W.; Yao, Y., Quantum spin Hall effect in silicene and two-dimensional germanium. *Phys. Rev. Lett.* **2011,** 107, 7, 076802.
17. Schaibley, J. R.; Yu, H.; Clark, G.; Rivera, P.; Ross, J. S.; Seyler, K. L.; Yao, W.; Xu, X., Valleytronics in 2D materials. *Nat. Rev. Mater.* **2016,** 1, 11, 1-15.
18. Castellanos-Gomez, A., Why all the fuss about 2D semiconductors? *Nat. Photonics* **2016,** 10, 4, 202-204.
19. Xu, M.; Liang, T.; Shi, M.; Chen, H., Graphene-like two-dimensional materials. *Chem. Rev.* **2013,** 113, 5, 3766-3798.
20. Aufray, B.; Kara, A.; Vizzini, S.; Oughaddou, H.; Léandri, C.; Ealet, B.; Le Lay, G., Graphene-like silicon nanoribbons on Ag (110): A possible formation of silicene. *Appl. Phys. Lett.* **2010,** 96, 18, 183102.
21. Dávila, M.; Xian, L.; Cahangirov, S.; Rubio, A.; Le Lay, G., Germanene: a novel two-dimensional germanium allotrope akin to graphene and silicene. *New J. Phys.* **2014,** 16, 9, 095002.
22. Mannix, A. J.; Zhou, X.-F.; Kiraly, B.; Wood, J. D.; Alducin, D.; Myers, B. D.; Liu, X.; Fisher, B. L.; Santiago, U.; Guest, J. R., Synthesis of borophenes: Anisotropic, two-dimensional boron polymorphs. *Science* **2015,** 350, 6267, 1513-1516.
23. Li, L.; Yu, Y.; Ye, G. J.; Ge, Q.; Ou, X.; Wu, H.; Feng, D.; Chen, X. H.; Zhang, Y., Black phosphorus field-effect transistors. *Nat. Nanotechnol.* **2014,** 9, 5, 372-377.
24. Zhang, S.; Yan, Z.; Li, Y.; Chen, Z.; Zeng, H., Atomically thin arsenene and antimonene: semimetal–semiconductor and indirect–direct band-gap transitions. *Angew. Chem.* **2015,** 127, 10, 3155-3158.
25. Zhu, F.-f.; Chen, W.-j.; Xu, Y.; Gao, C.-l.; Guan, D.-d.; Liu, C.-h.; Qian, D.; Zhang, S.-C.; Jia, J.-f., Epitaxial growth of two-dimensional stanene. *Nat. Mater.* **2015,** 14, 10, 1020-1025.
26. Reis, F.; Li, G.; Dudy, L.; Bauernfeind, M.; Glass, S.; Hanke, W.; Thomale, R.; Schäfer, J.; Claessen, R., Bismuthene on a SiC substrate: A candidate for a high-temperature quantum spin Hall material. *Science* **2017,** 357, 6348, 287-290.
27. Zhu, Z.; Cai, X.; Yi, S.; Chen, J.; Dai, Y.; Niu, C.; Guo, Z.; Xie, M.; Liu, F.; Cho, J.-H., Multivalency-driven formation of Te-based monolayer materials: a combined first-principles and experimental study. *Phys. Rev. Lett.* **2017,** 119, 10, 106101.
28. Qin, J.; Qiu, G.; Jian, J.; Zhou, H.; Yang, L.; Charnas, A.; Zemlyanov, D. Y.; Xu, C.-Y.; Xu, X.; Wu, W., Controlled growth of a large-size 2D selenium nanosheet and its electronic and optoelectronic applications. *ACS Nano* **2017,** 11, 10, 10222-10229.

29. Kochat, V.; Samanta, A.; Zhang, Y.; Bhowmick, S.; Manimunda, P.; Asif, S. A. S.; Stender, A. S.; Vajtai, R.; Singh, A. K.; Tiwary, C. S., Atomically thin gallium layers from solid-melt exfoliation. *Sci. Adv.* **2018,** 4, 3, e1701373.
30. Yuhara, J.; He, B.; Matsunami, N.; Nakatake, M.; Le Lay, G., Graphene's latest cousin: Plumbene epitaxial growth on a "nano WaterCube". *Adv. Mater.* **2019,** 31, 27, 1901017.
31. Yeoh, K. H.; Yoon, T. L.; Ong, D. S.; Lim, T. L., First-principles studies on the superconductivity of aluminene. *Appl. Surf. Sci.* **2018,** 445, 161-166.
32. Liu, G.; Xu, S.-G.; Ma, Y.; Shao, X.; Xiong, W.; Wu, X.; Zhang, S.; Liao, C.; Chen, C.; Wang, X., Arsenic Monolayers Formed by Zero-Dimensional Tetrahedral Clusters and One-Dimensional Armchair Nanochains. *ACS Nano* **2022**.
33. Hernandez, Y.; Nicolosi, V.; Lotya, M.; Blighe, F. M.; Sun, Z.; De, S.; McGovern, I. T.; Holland, B.; Byrne, M.; Gun'Ko, Y. K., High-yield production of graphene by liquid-phase exfoliation of graphite. *Nat. Nanotechnol.* **2008,** 3, 9, 563-568.
34. Ni, Z.; Ma, L.; Du, S.; Xu, Y.; Yuan, M.; Fang, H.; Wang, Z.; Xu, M.; Li, D.; Yang, J., Plasmonic silicon quantum dots enabled high-sensitivity ultrabroadband photodetection of graphene-based hybrid phototransistors. *ACS Nano* **2017,** 11, 10, 9854-9862.
35. Chen, X.; Liu, X.; Wu, B.; Nan, H.; Guo, H.; Ni, Z.; Wang, F.; Wang, X.; Shi, Y.; Wang, X., Improving the performance of graphene phototransistors using a heterostructure as the light-absorbing layer. *Nano Lett.* **2017,** 17, 10, 6391-6396.
36. Kim, M.; Safron, N. S.; Huang, C.; Arnold, M. S.; Gopalan, P., Light-driven reversible modulation of doping in graphene. *Nano Lett.* **2012,** 12, 1, 182-187.
37. Cai, J.; Pignedoli, C. A.; Talirz, L.; Ruffieux, P.; Söde, H.; Liang, L.; Meunier, V.; Berger, R.; Li, R.; Feng, X., Graphene nanoribbon heterojunctions. *Nat. Nanotechnol.* **2014,** 9, 11, 896-900.
38. Zhu, H.; Gan, X.; McCreary, A.; Lv, R.; Lin, Z.; Terrones, M., Heteroatom doping of two-dimensional materials: from graphene to chalcogenides. *Nano Today* **2020,** 30, 100829.
39. de la Torre, B.; Švec, M.; Hapala, P.; Redondo, J.; Krejčí, O.; Lo, R.; Manna, D.; Sarmah, A.; Nachtigallová, D.; Tuček, J., Non-covalent control of spin-state in metal-organic complex by positioning on N-doped graphene. *Nat. Commun.* **2018,** 9, 1, 1-9.
40. Wehling, T.; Novoselov, K.; Morozov, S.; Vdovin, E.; Katsnelson, M.; Geim, A.; Lichtenstein, A., Molecular doping of graphene. *Nano Lett.* **2008,** 8, 1, 173-177.
41. Gong, Y.; Lin, J.; Wang, X.; Shi, G.; Lei, S.; Lin, Z.; Zou, X.; Ye, G.; Vajtai, R.; Yakobson, B. I., Vertical and in-plane heterostructures from WS2/MoS2 monolayers. *Nat. Mater.* **2014,** 13, 12, 1135-1142.
42. Liu, Z.; Ma, L.; Shi, G.; Zhou, W.; Gong, Y.; Lei, S.; Yang, X.; Zhang, J.; Yu, J.; Hackenberg, K. P., In-plane heterostructures of graphene and hexagonal boron nitride with controlled domain sizes. *Nat. Nanotechnol.* **2013,** 8, 2, 119-124.
43. Chen, K.; Wan, X.; Xie, W.; Wen, J.; Kang, Z.; Zeng, X.; Chen, H.; Xu, J., Lateral built-in potential of monolayer MoS2–WS2 in-plane heterostructures by a shortcut growth strategy. *Adv. Mater.* **2015,** 27, 41, 6431-6437.
44. Sangwan, V. K.; Jariwala, D.; Kim, I. S.; Chen, K.-S.; Marks, T. J.; Lauhon, L. J.; Hersam, M. C., Gate-tunable memristive phenomena mediated by grain boundaries in single-layer MoS2. *Nat. Nanotechnol.* **2015,** 10, 5, 403-406.
45. Ruffieux, P.; Wang, S.; Yang, B.; Sánchez-Sánchez, C.; Liu, J.; Dienel, T.; Talirz, L.; Shinde, P.; Pignedoli, C. A.; Passerone, D., On-surface synthesis of graphene nanoribbons with zigzag edge topology. *Nature* **2016,** 531, 7595, 489-492.
46. Yang, L.; Cohen, M. L.; Louie, S. G., Magnetic edge-state excitons in zigzag graphene nanoribbons. *Phys. Rev. Lett.* **2008,** 101, 18, 186401.
47. Jacobberger, R. M.; Kiraly, B.; Fortin-Deschenes, M.; Levesque, P. L.; McElhinny, K. M.; Brady, G. J.; Rojas Delgado, R.; Singha Roy, S.; Mannix, A.; Lagally, M. G., Direct oriented growth of armchair graphene nanoribbons on germanium. *Nat. Commun.* **2015,** 6, 1, 1-8.
48. Li, G.; Yoon, K.-Y.; Zhong, X.; Wang, J.; Zhang, R.; Guest, J. R.; Wen, J.; Zhu, X.-Y.; Dong, G., A modular synthetic approach for band-gap engineering of armchair graphene nanoribbons. *Nat. Commun.* **2018,** 9, 1, 1-9.
49. Cho, S.; Kim, S.; Kim, J. H.; Zhao, J.; Seok, J.; Keum, D. H.; Baik, J.; Choe, D.-H.; Chang, K. J.; Suenaga, K., Phase patterning for ohmic homojunction contact in MoTe2. *Science* **2015,** 349, 6248, 625-628.
50. Yang, S.; Chen, Y.; Jiang, C., Strain engineering of two-dimensional materials: methods, properties, and applications. *InfoMat* **2021,** 3, 4, 397-420.
51. Peng, X.; Wei, Q.; Copple, A., Strain-engineered direct-indirect band gap transition and its mechanism in two-dimensional phosphorene. *Phys. Rev. B* **2014,** 90, 8, 085402.
52. Cao, Y.; Fatemi, V.; Fang, S.; Watanabe, K.; Taniguchi, T.; Kaxiras, E.; Jarillo-Herrero, P., Unconventional superconductivity in magic-angle graphene superlattices. *Nature* **2018,** 556, 7699, 43-50.
53. Cao, Y.; Fatemi, V.; Demir, A.; Fang, S.; Tomarken, S. L.; Luo, J. Y.; Sanchez-Yamagishi, J. D.; Watanabe, K.; Taniguchi, T.; Kaxiras, E., Correlated insulator behaviour at half-filling in magic-angle graphene superlattices. *Nature* **2018,** 556, 7699, 80-84.
54. Peng, B.; Zhang, H.; Shao, H.; Ning, Z.; Xu, Y.; Ni, G.; Lu, H.; Zhang, D. W.; Zhu, H., Stability and strength of atomically thin borophene from first principles calculations. *Materials Research Letters* **2017,** 5, 6, 399-407.
55. Yuan, J.; Yu, N.; Xue, K.; Miao, X., Stability, electronic and thermodynamic properties of aluminene from first-principles calculations. *Appl. Surf. Sci.* **2017,** 409, 85-90.
56. Mardanya, S.; Thakur, V. K.; Bhowmick, S.; Agarwal, A., Four allotropes of semiconducting layered arsenic that switch into a topological insulator via an electric field: Computational study. *Phys. Rev. B* **2016,** 94, 3, 035423.
57. Matusalem, F.; Marques, M.; Teles, L. K.; Bechstedt, F., Stability and electronic structure of two-dimensional allotropes of group-IV materials. *Phys. Rev. B* **2015,** 92, 4, 045436.

58. Xian, L.; Paz, A. P.; Bianco, E.; Ajayan, P. M.; Rubio, A., Square selenene and tellurene: novel group VI elemental 2D materials with nontrivial topological properties. *2D Mater.* **2017,** 4, 4, 041003.
59. Zhang, Z.; Yang, Y.; Gao, G.; Yakobson, B. I., Two-dimensional boron monolayers mediated by metal substrates. *Angew. Chem.* **2015,** 127, 44, 13214-13218.
60. Liu, Y.; Penev, E. S.; Yakobson, B. I., Probing the synthesis of two-dimensional boron by first-principles computations. *Angew. Chem., Int. Ed.* **2013,** 52, 11, 3156-3159.
61. Huang, Y.; Shirodkar, S. N.; Yakobson, B. I., Two-dimensional boron polymorphs for visible range plasmonics: a first-principles exploration. *J. Am. Chem. Soc.* **2017,** 139, 47, 17181-17185.
62. Singh, D.; Gupta, S. K.; Lukačević, I.; Sonvane, Y., Indiene 2D monolayer: a new nanoelectronic material. *RSC adv.* **2016,** 6, 10, 8006-8014.
63. Deng, J.; Xia, B.; Ma, X.; Chen, H.; Shan, H.; Zhai, X.; Li, B.; Zhao, A.; Xu, Y.; Duan, W., Epitaxial growth of ultraflat stanene with topological band inversion. *Nat. Mater.* **2018,** 17, 12, 1081-1086.
64. Ren, W.; Cheng, H.-M., The global growth of graphene. *Nat. Nanotechnol.* **2014,** 9, 10, 726-730.
65. Sprinkle, M.; Ruan, M.; Hu, Y.; Hankinson, J.; Rubio-Roy, M.; Zhang, B.; Wu, X.; Berger, C.; De Heer, W. A., Scalable templated growth of graphene nanoribbons on SiC. *Nat. Nanotechnol.* **2010,** 5, 10, 727-731.
66. Meng, L.; Wang, Y.; Zhang, L.; Du, S.; Wu, R.; Li, L.; Zhang, Y.; Li, G.; Zhou, H.; Hofer, W. A., Buckled silicene formation on Ir (111). *Nano Lett.* **2013,** 13, 2, 685-690.
67. Li, L.; Lu, S. z.; Pan, J.; Qin, Z.; Wang, Y. q.; Wang, Y.; Cao, G. y.; Du, S.; Gao, H. J., Buckled germanene formation on Pt (111). *Adv. Mater.* **2014,** 26, 28, 4820-4824.
68. Zhang, S.; Zhou, J.; Wang, Q.; Chen, X.; Kawazoe, Y.; Jena, P., Penta-graphene: A new carbon allotrope. *Proc. Natl Acad. Sci. USA* **2015,** 112, 8, 2372-2377.
69. Wang, Z.; Zhou, X.-F.; Zhang, X.; Zhu, Q.; Dong, H.; Zhao, M.; Oganov, A. R., Phagraphene: a low-energy graphene allotrope composed of 5–6–7 carbon rings with distorted dirac cones. *Nano Lett.* **2015,** 15, 9, 6182-6186.
70. Guan, J.; Zhu, Z.; Tománek, D., Tiling phosphorene. *ACS Nano* **2014,** 8, 12, 12763-12768.
71. Wu, X.; Shao, Y.; Liu, H.; Feng, Z.; Wang, Y. L.; Sun, J. T.; Liu, C.; Wang, J. O.; Liu, Z. L.; Zhu, S. Y., Epitaxial growth and air-stability of monolayer antimonene on PdTe2. *Adv. Mater.* **2017,** 29, 11, 1605407.
72. Lu, Y.; Xu, W.; Zeng, M.; Yao, G.; Shen, L.; Yang, M.; Luo, Z.; Pan, F.; Wu, K.; Das, T., Topological properties determined by atomic buckling in self-assembled ultrathin Bi (110). *Nano Lett.* **2015,** 15, 1, 80-87.
73. Carvalho, A.; Wang, M.; Zhu, X.; Rodin, A. S.; Su, H.; Castro Neto, A. H., Phosphorene: from theory to applications. *Nat. Rev. Mater.* **2016,** 1, 11, 1-16.
74. Aktürk, E.; Aktürk, O. Ü.; Ciraci, S., Single and bilayer bismuthene: Stability at high temperature and mechanical and electronic properties. *Phys. Rev. B* **2016,** 94, 1, 014115.
75. Kamal, C.; Ezawa, M., Arsenene: Two-dimensional buckled and puckered honeycomb arsenic systems. *Phys. Rev. B* **2015,** 91, 8, 085423.
76. Feng, B.; Zhang, J.; Zhong, Q.; Li, W.; Li, S.; Li, H.; Cheng, P.; Meng, S.; Chen, L.; Wu, K., Experimental realization of two-dimensional boron sheets. *Nat. Chem.* **2016,** 8, 6, 563-568.
77. Li, W.; Kong, L.; Chen, C.; Gou, J.; Sheng, S.; Zhang, W.; Li, H.; Chen, L.; Cheng, P.; Wu, K., Experimental realization of honeycomb borophene. *Sci. Bull.* **2018,** 63, 5, 282-286.
78. Kiraly, B.; Liu, X.; Wang, L.; Zhang, Z.; Mannix, A. J.; Fisher, B. L.; Yakobson, B. I.; Hersam, M. C.; Guisinger, N. P., Borophene synthesis on Au (111). *ACS Nano* **2019,** 13, 4, 3816-3822.
79. Zhang, Z.; Yang, Y.; Penev, E. S.; Yakobson, B. I., Elasticity, flexibility, and ideal strength of borophenes. *Adv. Funct. Mater.* **2017,** 27, 9, 1605059.
80. Zhao, Y.; Zeng, S.; Ni, J., Superconductivity in two-dimensional boron allotropes. *Phys. Rev. B* **2016,** 93, 1, 014502.
81. Zhang, Z.; Penev, E. S.; Yakobson, B. I., Polyphony in B flat. *Nat. Chem.* **2016,** 8, 6, 525-527.
82. Penev, E. S.; Bhowmick, S.; Sadrzadeh, A.; Yakobson, B. I., Polymorphism of two-dimensional boron. *Nano Lett.* **2012,** 12, 5, 2441-2445.
83. Wang, Z.; Lü, T.-Y.; Wang, H.-Q.; Feng, Y. P.; Zheng, J.-C., High anisotropy of fully hydrogenated borophene. *Phys. Chem. Chem. Phys.* **2016,** 18, 46, 31424-31430.
84. Wang, H.; Li, Q.; Gao, Y.; Miao, F.; Zhou, X.-F.; Wan, X., Strain effects on borophene: ideal strength, negative Possion's ratio and phonon instability. *New J. Phys.* **2016,** 18, 7, 073016.
85. Peköz, R.; Konuk, M.; Kilic, M. E.; Durgun, E., Two-dimensional fluorinated boron sheets: mechanical, electronic, and thermal properties. *ACS Omega* **2018,** 3, 2, 1815-1822.
86. Zhou, Y.-P.; Jiang, J.-W., Molecular dynamics simulations for mechanical properties of borophene: parameterization of valence force field model and Stillinger-Weber potential. *Sci. Rep.* **2017,** 7, 1, 1-12.
87. Le, M. Q.; Mortazavi, B.; Rabczuk, T., Mechanical properties of borophene films: a reactive molecular dynamics investigation. *Nanotechnology* **2016,** 27, 44, 445709.
88. Zhong, H.; Huang, K.; Yu, G.; Yuan, S., Electronic and mechanical properties of few-layer borophene. *Phys. Rev. B* **2018,** 98, 5, 054104.
89. Mortazavi, B.; Rahaman, O.; Dianat, A.; Rabczuk, T., Mechanical responses of borophene sheets: a first-principles study. *Phys. Chem. Chem. Phys.* **2016,** 18, 39, 27405-27413.

90. Zhou, H.; Cai, Y.; Zhang, G.; Zhang, Y.-W., Superior lattice thermal conductance of single-layer borophene. *NPJ 2D Mater. Appl.* **2017,** 1, 1, 1-7.
91. Li, D.; He, J.; Ding, G.; Tang, Q.; Ying, Y.; He, J.; Zhong, C.; Liu, Y.; Feng, C.; Sun, Q., Stretch-driven increase in ultrahigh thermal conductance of hydrogenated borophene and dimensionality crossover in phonon transmission. *Adv. Funct. Mater.* **2018,** 28, 31, 1801685.
92. Kong, L.; Liu, L.; Chen, L.; Zhong, Q.; Cheng, P.; Li, H.; Zhang, Z.; Wu, K., One-dimensional nearly free electron states in borophene. *Nanoscale* **2019,** 11, 33, 15605-15611.
93. Feng, B.; Zhang, J.; Liu, R.-Y.; Iimori, T.; Lian, C.; Li, H.; Chen, L.; Wu, K.; Meng, S.; Komori, F., Direct evidence of metallic bands in a monolayer boron sheet. *Phys. Rev. B* **2016,** 94, 4, 041408.
94. Zhou, X.-F.; Dong, X.; Oganov, A. R.; Zhu, Q.; Tian, Y.; Wang, H.-T., Semimetallic two-dimensional boron allotrope with massless Dirac fermions. *Phys. Rev. Lett.* **2014,** 112, 8, 085502.
95. Feng, B.; Sugino, O.; Liu, R.-Y.; Zhang, J.; Yukawa, R.; Kawamura, M.; Iimori, T.; Kim, H.; Hasegawa, Y.; Li, H., Dirac fermions in borophene. *Phys. Rev. Lett.* **2017,** 118, 9, 096401.
96. Shukla, V.; Grigoriev, A.; Jena, N. K.; Ahuja, R., Strain controlled electronic and transport anisotropies in two-dimensional borophene sheets. *Phys. Chem. Chem. Phys.* **2018,** 20, 35, 22952-22960.
97. Wang, Z.-Q.; Lü, T.-Y.; Wang, H.-Q.; Feng, Y. P.; Zheng, J.-C., Band structure engineering of borophane by first principles calculations. *RSC adv.* **2017,** 7, 75, 47746-47752.
98. Gao, M.; Li, Q.-Z.; Yan, X.-W.; Wang, J., Prediction of phonon-mediated superconductivity in borophene. *Phys. Rev. B* **2017,** 95, 2, 024505.
99. Zhao, Y.; Zeng, S.; Ni, J., Phonon-mediated superconductivity in borophenes. *Appl. Phys. Lett.* **2016,** 108, 24, 242601.
100. Zhao, Y.; Zeng, S.; Lian, C.; Dai, Z.; Meng, S.; Ni, J., Multigap anisotropic superconductivity in borophenes. *Phys. Rev. B* **2018,** 98, 13, 134514.
101. Penev, E. S.; Kutana, A.; Yakobson, B. I., Can two-dimensional boron superconduct? *Nano Lett.* **2016,** 16, 4, 2522-2526.
102. Liao, J.-H.; Zhao, Y.-C.; Zhao, Y.-J.; Xu, H.; Yang, X.-B., Phonon-mediated superconductivity in Mg intercalated bilayer borophenes. *Phys. Chem. Chem. Phys.* **2017,** 19, 43, 29237-29243.
103. Li, G.; Zhao, Y.; Zeng, S.; Zulfiqar, M.; Ni, J., Strain effect on the superconductivity in borophenes. *J. Phys. Chem. C* **2018,** 122, 29, 16916-16924.
104. Cheng, C.; Sun, J.-T.; Liu, H.; Fu, H.-X.; Zhang, J.; Chen, X.-R.; Meng, S., Suppressed superconductivity in substrate-supported β12 borophene by tensile strain and electron doping. *2D Mater.* **2017,** 4, 2, 025032.
105. Zheng, J.-C.; Zhu, Y., Searching for a higher superconducting transition temperature in strained Mg B 2. *Phys. Rev. B* **2006,** 73, 2, 024509.
106. Xiao, R.; Shao, D.; Lu, W.; Lv, H.; Li, J.; Sun, Y., Enhanced superconductivity by strain and carrier-doping in borophene: A first principles prediction. *Appl. Phys. Lett.* **2016,** 109, 12, 122604.
107. Jiao, Y.; Ma, F.; Bell, J.; Bilic, A.; Du, A., Two-Dimensional Boron Hydride Sheets: High Stability, Massless Dirac Fermions, and Excellent Mechanical Properties. *Angew. Chem.* **2016,** 128, 35, 10448-10451.
108. Nishino, H.; Fujita, T.; Cuong, N. T.; Tominaka, S.; Miyauchi, M.; Iimura, S.; Hirata, A.; Umezawa, N.; Okada, S.; Nishibori, E., Formation and characterization of hydrogen boride sheets derived from MgB2 by cation exchange. *J. Am. Chem. Soc.* **2017,** 139, 39, 13761-13769.
109. Wang, C.-B.; Lu, Q.; Zhang, L.-L.; Xu, T.-T.; Gong, W.-J., Li-decorated borophene–graphene heterostructure under gas adsorption. *J. Phys. Chem. Solids* **2022,** 171, 111033.
110. Tao, M.-L.; Tu, Y.-B.; Sun, K.; Wang, Y.-L.; Xie, Z.-B.; Liu, L.; Shi, M.-X.; Wang, J.-Z., Gallenene epitaxially grown on Si (111). *2D Mater.* **2018,** 5, 3, 035009.
111. Zhang, H.-M.; Sun, Y.; Li, W.; Peng, J.-P.; Song, C.-L.; Xing, Y.; Zhang, Q.; Guan, J.; Li, Z.; Zhao, Y., Detection of a superconducting phase in a two-atom layer of hexagonal Ga film grown on semiconducting GaN (0001). *Phys. Rev. Lett.* **2015,** 114, 10, 107003.
112. Gruznev, D.; Bondarenko, L.; Tupchaya, A.; Mihalyuk, A.; Eremeev, S.; Zotov, A.; Saranin, A., Thallene: graphene-like honeycomb lattice of Tl atoms frozen on single-layer NiSi2. *2D Mater.* **2020,** 7, 4, 045026.
113. Neto, A. C.; Guinea, F.; Peres, N. M.; Novoselov, K. S.; Geim, A. K., The electronic properties of graphene. *Rev. Mod. Phys.* **2009,** 81, 1, 109.
114. Lonkar, S. P.; Deshmukh, Y. S.; Abdala, A. A., Recent advances in chemical modifications of graphene. *Nano Research* **2015,** 8, 4, 1039-1074.
115. Geim, A. K.; Novoselov, K. S., The rise of graphene. *Nat. Mater.* **2007,** 6, 3, 183-191.
116. Nair, R. R.; Blake, P.; Grigorenko, A. N.; Novoselov, K. S.; Booth, T. J.; Stauber, T.; Peres, N. M.; Geim, A. K., Fine structure constant defines visual transparency of graphene. *Science* **2008,** 320, 5881, 1308-1308.
117. Balandin, A. A.; Ghosh, S.; Bao, W.; Calizo, I.; Teweldebrhan, D.; Miao, F.; Lau, C. N., Superior thermal conductivity of single-layer graphene. *Nano Lett.* **2008,** 8, 3, 902-907.
118. Guo, B.; Liu, Q.; Chen, E.; Zhu, H.; Fang, L.; Gong, J. R., Controllable N-doping of graphene. *Nano Lett.* **2010,** 10, 12, 4975-4980.
119. Wang, H.; Zhou, Y.; Wu, D.; Liao, L.; Zhao, S.; Peng, H.; Liu, Z., Synthesis of boron-doped graphene monolayers using the sole solid feedstock by chemical vapor deposition. *Small* **2013,** 9, 8, 1316-1320.
120. Jang, A.-R.; Jeon, E. K.; Kang, D.; Kim, G.; Kim, B.-S.; Kang, D. J.; Shin, H. S., Reversibly light-modulated dirac point of graphene functionalized with spiropyran. *ACS Nano* **2012,** 6, 10, 9207-9213.

121. Levendorf, M. P.; Kim, C.-J.; Brown, L.; Huang, P. Y.; Havener, R. W.; Muller, D. A.; Park, J., Graphene and boron nitride lateral heterostructures for atomically thin circuitry. *Nature* **2012,** 488, 7413, 627-632.
122. Takeda, K.; Shiraishi, K., Theoretical possibility of stage corrugation in Si and Ge analogs of graphite. *Phys. Rev. B* **1994,** 50, 20, 14916.
123. Cahangirov, S.; Topsakal, M.; Aktürk, E.; Şahin, H.; Ciraci, S., Two-and one-dimensional honeycomb structures of silicon and germanium. *Phys. Rev. Lett.* **2009,** 102, 23, 236804.
124. Ryu, S.; Hatsugai, Y., Topological origin of zero-energy edge states in particle-hole symmetric systems. *Phys. Rev. Lett.* **2002,** 89, 7, 077002.
125. Liu, C.-C.; Jiang, H.; Yao, Y., Low-energy effective Hamiltonian involving spin-orbit coupling in silicene and two-dimensional germanium and tin. *Phys. Rev. B* **2011,** 84, 19, 195430.
126. Xu, C.; Luo, G.; Liu, Q.; Zheng, J.; Zhang, Z.; Nagase, S.; Gao, Z.; Lu, J., Giant magnetoresistance in silicene nanoribbons. *Nanoscale* **2012,** 4, 10, 3111-3117.
127. Rachel, S.; Ezawa, M., Giant magnetoresistance and perfect spin filter in silicene, germanene, and stanene. *Phys. Rev. B* **2014,** 89, 19, 195303.
128. Ni, Z.; Liu, Q.; Tang, K.; Zheng, J.; Zhou, J.; Qin, R.; Gao, Z.; Yu, D.; Lu, J., Tunable bandgap in silicene and germanene. *Nano Lett.* **2012,** 12, 1, 113-118.
129. Drummond, N.; Zolyomi, V.; Fal'Ko, V., Electrically tunable band gap in silicene. *Phys. Rev. B* **2012,** 85, 7, 075423.
130. Bao, H.; Liao, W.; Guo, J.; Zhao, H.; Zhou, G., Terahertz electromagnetic response and its electric field manipulation of bulked silicene. *Laser Physics Letters* **2015,** 12, 9, 095902.
131. Molle, A.; Goldberger, J.; Houssa, M.; Xu, Y.; Zhang, S.-C.; Akinwande, D., Buckled two-dimensional Xene sheets. *Nat. Mater.* **2017,** 16, 2, 163-169.
132. Brumfiel, G., Sticky problem snares wonder material. *Nature* **2013,** 495, 7440, 152-153.
133. De Padova, P.; Ottaviani, C.; Quaresima, C.; Olivieri, B.; Imperatori, P.; Salomon, E.; Angot, T.; Quagliano, L.; Romano, C.; Vona, A., 24 h stability of thick multilayer silicene in air. *2D Mater.* **2014,** 1, 2, 021003.
134. Ni, Z.; Zhong, H.; Jiang, X.; Quhe, R.; Luo, G.; Wang, Y.; Ye, M.; Yang, J.; Shi, J.; Lu, J., Tunable band gap and doping type in silicene by surface adsorption: towards tunneling transistors. *Nanoscale* **2014,** 6, 13, 7609-7618.
135. Wang, Y.; Ding, Y., Strain-induced self-doping in silicene and germanene from first-principles. *Solid State Commun.* **2013,** 155, 6-11.
136. Li, S.; Ao, Z.; Zhu, J.; Ren, J.; Yi, J.; Wang, G.; Liu, W., Strain controlled ferromagnetic-antiferromagnetic transformation in Mn-doped silicene for information transformation devices. *J. Phys. Chem. Lett.* **2017,** 8, 7, 1484-1488.
137. Wang, X.-Q.; Li, H.-D.; Wang, J.-T., Induced ferromagnetism in one-side semihydrogenated silicene and germanene. *Phys. Chem. Chem. Phys.* **2012,** 14, 9, 3031-3036.
138. Du, Y.; Zhuang, J.; Wang, J.; Li, Z.; Liu, H.; Zhao, J.; Xu, X.; Feng, H.; Chen, L.; Wu, K., Quasi-freestanding epitaxial silicene on Ag (111) by oxygen intercalation. *Sci. Adv.* **2016,** 2, 7, e1600067.
139. Liu, H.; Han, N.; Zhao, J., Band gap opening in bilayer silicene by alkali metal intercalation. *J. Phys.: Condens. Matter* **2014,** 26, 47, 475303.
140. Feng, J.-w.; Liu, Y.-j.; Wang, H.-x.; Zhao, J.-x.; Cai, Q.-h.; Wang, X.-z., Gas adsorption on silicene: a theoretical study. *Comp. Mater. Sci.* **2014,** 87, 218-226.
141. Osborne, D. A.; Morishita, T.; Tawfik, S. A.; Yayama, T.; Spencer, M. J., Adsorption of toxic gases on silicene/Ag (111). *Phys. Chem. Chem. Phys.* **2019,** 21, 32, 17521-17537.
142. Ye, X.-S.; Shao, Z.-G.; Zhao, H.; Yang, L.; Wang, C.-L., Intrinsic carrier mobility of germanene is larger than graphene's: first-principle calculations. *RSC adv.* **2014,** 4, 41, 21216-21220.
143. Dávila, M. E.; Le Lay, G., Few layer epitaxial germanene: a novel two-dimensional Dirac material. *Sci. Rep.* **2016,** 6, 1, 1-9.
144. Hoat, D.; Nguyen, D. K.; Ponce-Perez, R.; Guerrero-Sanchez, J.; Van On, V.; Rivas-Silva, J.; Cocoletzi, G. H., Opening the germanene monolayer band gap using halogen atoms: An efficient approach studied by first-principles calculations. *Appl. Surf. Sci.* **2021,** 551, 149318.
145. Pang, Q.; Zhang, C.-l.; Li, L.; Fu, Z.-q.; Wei, X.-m.; Song, Y.-l., Adsorption of alkali metal atoms on germanene: A first-principles study. *Appl. Surf. Sci.* **2014,** 314, 15-20.
146. Jiao, Z.; Yao, Q.; Rudenko, A.; Zhang, L.; Zandvliet, H., Germanium/MoS2: Competition between the growth of germanene and intercalation. *Phys. Rev. B* **2020,** 102, 20, 205419.
147. Kaloni, T. P., Tuning the structural, electronic, and magnetic properties of germanene by the adsorption of 3d transition metal atoms. *J. Phys. Chem. C* **2014,** 118, 43, 25200-25208.
148. Sun, M.; Ren, Q.; Wang, S.; Zhang, Y.; Du, Y.; Yu, J.; Tang, W., Magnetism in transition-metal-doped germanene: a first-principles study. *Comp. Mater. Sci.* **2016,** 118, 112-116.
149. Lin, C.-H.; Huang, A.; Pai, W. W.; Chen, W.-C.; Chen, T.-Y.; Chang, T.-R.; Yukawa, R.; Cheng, C.-M.; Mou, C.-Y.; Matsuda, I., Single-layer dual germanene phases on Ag(111). *Phys. Rev. Mater.* **2018,** 2, 2, 024003.
150. Yuhara, J.; Shimazu, H.; Ito, K.; Ohta, A.; Araidai, M.; Kurosawa, M.; Nakatake, M.; Le Lay, G., Germanene epitaxial growth by segregation through Ag (111) thin films on Ge (111). *ACS Nano* **2018,** 12, 11, 11632-11637.
151. Muzychenko, D. A.; Oreshkin, S. I.; Panov, V. I.; Van Haesendonck, C.; Oreshkin, A. I., Single and multi domain buckled germanene phases on Al (111) surface. *Nano Research* **2019,** 12, 12, 2988-2996.

152. Zhang, L.; Bampoulis, P.; Rudenko, A.; Yao, Q. v.; Van Houselt, A.; Poelsema, B.; Katsnelson, M.; Zandvliet, H., Structural and electronic properties of germanene on MoS 2. *Phys. Rev. Lett.* **2016,** 116, 25, 256804.
153. Zhuang, J.; Gao, N.; Li, Z.; Xu, X.; Wang, J.; Zhao, J.; Dou, S. X.; Du, Y., Cooperative electron–phonon coupling and buckled structure in germanene on Au (111). *ACS Nano* **2017,** 11, 4, 3553-3559.
154. Xu, Y.; Yan, B.; Zhang, H.-J.; Wang, J.; Xu, G.; Tang, P.; Duan, W.; Zhang, S.-C., Large-gap quantum spin Hall insulators in tin films. *Phys. Rev. Lett.* **2013,** 111, 13, 136804.
155. Fu, L.; Kane, C. L.; Mele, E. J., Topological insulators in three dimensions. *Phys. Rev. Lett.* **2007,** 98, 10, 106803.
156. Chen, X.; Tan, C.; Yang, Q.; Meng, R.; Liang, Q.; Cai, M.; Zhang, S.; Jiang, J., Ab initio study of the adsorption of small molecules on stanene. *J. Phys. Chem. C* **2016,** 120, 26, 13987-13994.
157. Monshi, M. M.; Aghaei, S. M.; Calizo, I., Doping and defect-induced germanene: A superior media for sensing H2S, SO2, and CO2 gas molecules. *Surf. Sci.* **2017,** 665, 96-102.
158. Xiong, W.; Xia, C.; Peng, Y.; Du, J.; Wang, T.; Zhang, J.; Jia, Y., Spin–orbit coupling effects on electronic structures in stanene nanoribbons. *Phys. Chem. Chem. Phys.* **2016,** 18, 9, 6534-6540.
159. Shaidu, Y.; Akin-Ojo, O., First principles predictions of superconductivity in doped stanene. *Comp. Mater. Sci.* **2016,** 118, 11-15.
160. Zhao, H.; Zhang, C.-w.; Ji, W.-x.; Zhang, R.-w.; Li, S.-s.; Yan, S.-s.; Zhang, B.-m.; Li, P.; Wang, P.-j., Unexpected giant-gap quantum spin Hall insulator in chemically decorated plumbene monolayer. *Sci. Rep.* **2016,** 6, 1, 1-8.
161. Yu, X.-L.; Wu, J., Evolution of the topological properties of two-dimensional group IVA materials and device design. *Phys. Chem. Chem. Phys.* **2018,** 20, 4, 2296-2307.
162. Yu, X.-L.; Huang, L.; Wu, J., From a normal insulator to a topological insulator in plumbene. *Phys. Rev. B* **2017,** 95, 12, 125113.
163. Hashemi, D.; Iizuka, H., Magnetic properties of 3d transition metal (Sc–Ni) doped plumbene. *RSC adv.* **2020,** 10, 12, 6884-6892.
164. Bihlmayer, G.; Sassmannshausen, J.; Kubetzka, A.; Blügel, S.; von Bergmann, K.; Wiesendanger, R., Plumbene on a magnetic substrate: a combined scanning tunneling microscopy and density functional theory study. *Phys. Rev. Lett.* **2020,** 124, 12, 126401.
165. Zhang, S.; Guo, S.; Chen, Z.; Wang, Y.; Gao, H.; Gómez-Herrero, J.; Ares, P.; Zamora, F.; Zhu, Z.; Zeng, H., Recent progress in 2D group-VA semiconductors: from theory to experiment. *Chem. Soc. Rev.* **2018,** 47, 3, 982-1021.
166. Batmunkh, M.; Bat-Erdene, M.; Shapter, J. G., Phosphorene and phosphorene-based materials–prospects for future applications. *Adv. Mater.* **2016,** 28, 39, 8586-8617.
167. Hashmi, A.; Hong, J., Transition metal doped phosphorene: first-principles study. *J. Phys. Chem. C* **2015,** 119, 17, 9198-9204.
168. Liu, Y.; Liu, C.; Wang, J.; Gao, Q.; Hu, Z.; Hao, W.; Xu, X.; Du, Y.; Zhuang, J., Reversible Potassium Intercalation in Blue Phosphorene–Au Network Driven by an Electric Field. *J. Phys. Chem. Lett.* **2020,** 11, 14, 5584-5590.
169. Liu, Q.; Zhang, X.; Abdalla, L.; Fazzio, A.; Zunger, A., Switching a normal insulator into a topological insulator via electric field with application to phosphorene. *Nano Lett.* **2015,** 15, 2, 1222-1228.
170. Wei, Z.; Zhang, Y.; Wang, S.; Wang, C.; Ma, J., Fe-doped phosphorene for the nitrogen reduction reaction. *J. Mater. Chem. A* **2018,** 6, 28, 13790-13796.
171. Xu, G.; Li, H.; Bati, A. S.; Bat-Erdene, M.; Nine, M. J.; Losic, D.; Chen, Y.; Shapter, J. G.; Batmunkh, M.; Ma, T., Nitrogen-doped phosphorene for electrocatalytic ammonia synthesis. *J. Mater. Chem. A* **2020,** 8, 31, 15875-15883.
172. Safari, F.; Moradinasab, M.; Fathipour, M.; Kosina, H., Adsorption of the NH3, NO, NO2, CO2, and CO gas molecules on blue phosphorene: a first-principles study. *Appl. Surf. Sci.* **2019,** 464, 153-161.
173. Sisakht, E. T.; Fazileh, F.; Zare, M.; Zarenia, M.; Peeters, F., Strain-induced topological phase transition in phosphorene and in phosphorene nanoribbons. *Phys. Rev. B* **2016,** 94, 8, 085417.
174. Hu, Y.; Liang, J.; Xia, Y.; Zhao, C.; Jiang, M.; Ma, J.; Tie, Z.; Jin, Z., 2D arsenene and arsenic materials: Fundamental properties, preparation, and applications. *Small* **2022,** 18, 9, 2104556.
175. Shah, J.; Wang, W.; Sohail, H. M.; Uhrberg, R., Experimental evidence of monolayer arsenene: an exotic 2D semiconducting material. *2D Mater.* **2020,** 7, 2, 025013.
176. Zhang, H.; Ma, Y.; Chen, Z., Quantum spin hall insulators in strain-modified arsenene. *Nanoscale* **2015,** 7, 45, 19152-19159.
177. Kong, X.; Gao, M.; Yan, X.-W.; Lu, Z.-Y.; Xiang, T., Superconductivity in electron-doped arsenene. *Chinese Phys. B* **2018,** 27, 4, 046301.
178. Sheng, F.; Hua, C.; Cheng, M.; Hu, J.; Sun, X.; Tao, Q.; Lu, H.; Lu, Y.; Zhong, M.; Watanabe, K., Rashba valleys and quantum Hall states in few-layer black arsenic. *Nature* **2021,** 593, 7857, 56-60.
179. Som, N. N.; Mankad, V.; Jha, P. K., Hydrogen evolution reaction: The role of arsenene nanosheet and dopant. *Int. J. Hydrogen Energy* **2018,** 43, 47, 21634-21641.
180. Sun, M.; Wang, S.; Du, Y.; Yu, J.; Tang, W., Transition metal doped arsenene: a first-principles study. *Appl. Surf. Sci.* **2016,** 389, 594-600.
181. Xu, Y.; Peng, B.; Zhang, H.; Shao, H.; Zhang, R.; Zhu, H., First-principle calculations of optical properties of monolayer arsenene and antimonene allotropes. *Ann. Phys.-Berlin* **2017,** 529, 4, 1600152.
182. Zhang, S.; Xie, M.; Li, F.; Yan, Z.; Li, Y.; Kan, E.; Liu, W.; Chen, Z.; Zeng, H., Semiconducting group 15 monolayers: a broad range of band gaps and high carrier mobilities. *Angew. Chem.* **2016,** 128, 5, 1698-1701.
183. Batool, S.; Idrees, M.; Han, S. T.; Zhou, Y., 2D Layers of Group VA Semiconductors: Fundamental Properties and Potential Applications. *Adv. Sci.* **2022**, 2203956.
184. Pumera, M.; Sofer, Z., 2D monoelemental arsenene, antimonene, and bismuthene: beyond black phosphorus. *Adv. Mater.* **2017,** 29, 21, 1605299.

185. Ares, P.; Palacios, J. J.; Abellán, G.; Gómez-Herrero, J.; Zamora, F., Recent progress on antimonene: a new bidimensional material. *Adv. Mater.* **2018,** 30, 2, 1703771.
186. Yang, L.; Song, Y.; Mi, W.; Wang, X., Prediction of spin-dependent electronic structure in 3 d-transition-metal doped antimonene. *Appl. Phys. Lett.* **2016,** 109, 2, 022103.
187. Qi, M.; Dai, S.; Wu, P., Prediction of electronic and magnetic properties in 3d-transition-metal X-doped bismuthene (X= V, Cr, Mn and Fe). *Appl. Surf. Sci.* **2019,** 486, 58-64.
188. Yang, L.; Song, Y.; Mi, W.; Wang, X., The electronic structure and spin–orbit-induced spin splitting in antimonene with vacancy defects. *RSC adv.* **2016,** 6, 70, 66140-66146.
189. Zhang, J.-J.; Zhang, Y.; Dong, S., Protective layer enhanced the stability and superconductivity of tailored antimonene bilayer. *Phys. Rev. Mater.* **2018,** 2, 12, 126004.
190. Xie, M.; Zhang, S.; Cai, B.; Zou, Y.; Zeng, H., N-and p-type doping of antimonene. *RSC adv.* **2016,** 6, 18, 14620-14625.
191. Zhao, M.; Zhang, X.; Li, L., Strain-driven band inversion and topological aspects in Antimonene. *Sci. Rep.* **2015,** 5, 1, 1-7.
192. Liu, M.-Y.; Huang, Y.; Chen, Q.-Y.; Li, Z.-Y.; Cao, C.; He, Y., Strain and electric field tunable electronic structure of buckled bismuthene. *RSC adv.* **2017,** 7, 63, 39546-39555.
193. Liu, C.; Hu, T.; Wu, Y.; Gao, H.; Yang, Y.; Ren, W., 2D selenium allotropes from first principles and swarm intelligence. *J. Phys.: Condens. Matter* **2019,** 31, 23, 235702.
194. Singh, J.; Jamdagni, P.; Jakhar, M.; Kumar, A., Stability, electronic and mechanical properties of chalcogen (Se and Te) monolayers. *Phys. Chem. Chem. Phys.* **2020,** 22, 10, 5749-5755.
195. Zhang, W.; Wu, Q.; Yazyev, O. V.; Weng, H.; Guo, Z.; Cheng, W.-D.; Chai, G.-L., Topological phase transitions driven by strain in monolayer tellurium. *Phys. Rev. B* **2018,** 98, 11, 115411.
196. Zhu, W.; Yogeesh, M. N.; Yang, S.; Aldave, S. H.; Kim, J.-S.; Sonde, S.; Tao, L.; Lu, N.; Akinwande, D., Flexible black phosphorus ambipolar transistors, circuits and AM demodulator. *Nano Lett.* **2015,** 15, 3, 1883-1890.
197. Mayorga-Martinez, C. C.; Sofer, Z.; Pumera, M., Layered black phosphorus as a selective vapor sensor. *Angew. Chem., Int. Ed.* **2015,** 54, 48, 14317-14320.
198. Lin, S.; Liu, S.; Yang, Z.; Li, Y.; Ng, T. W.; Xu, Z.; Bao, Q.; Hao, J.; Lee, C. S.; Surya, C., Solution-processable ultrathin black phosphorus as an effective electron transport layer in organic photovoltaics. *Adv. Funct. Mater.* **2016,** 26, 6, 864-871.
199. Wu, S.; Fatemi, V.; Gibson, Q. D.; Watanabe, K.; Taniguchi, T.; Cava, R. J.; Jarillo-Herrero, P., Observation of the quantum spin Hall effect up to 100 kelvin in a monolayer crystal. *Science* **2018,** 359, 6371, 76-79.
200. Saito, Y.; Iizuka, T.; Koretsune, T.; Arita, R.; Shimizu, S.; Iwasa, Y., Gate-tuned thermoelectric power in black phosphorus. *Nano Lett.* **2016,** 16, 8, 4819-4824.
201. Yao, Y.; Fu, Q.; Zhang, Y.; Weng, X.; Li, H.; Chen, M.; Jin, L.; Dong, A.; Mu, R.; Jiang, P., Graphene cover-promoted metal-catalyzed reactions. *Proc. Natl Acad. Sci. USA* **2014,** 111, 48, 17023-17028.
202. Sakaguchi, H.; Song, S.; Kojima, T.; Nakae, T., Homochiral polymerization-driven selective growth of graphene nanoribbons. *Nat. Chem.* **2017,** 9, 1, 57-63.